HYDROCARBON POOL FIRE PERFORMANCE OF REINFORCED ELASTOMERIC BEARING PADS

by

SHASHANK MALAL

Presented to the Faculty of the Graduate School of

The University of Texas at Arlington in Partial Fulfillment

of the Requirements

for the Degree of

MASTER OF SCIENCE IN STRUCTURES AND APPLIED MECHANICS

THE UNIVERSITY OF TEXAS AT ARLINGTON

August 2017

Acknowledgements

I would like to express my sincere thanks to Dr. Nur Yazdani for his continuous support, guidance and mentorship. I am grateful to Dr. Shih-Ho Chao, Dr. Himan Hojat Jalai for accepting to serve on my dissertation committee and Dr. Eyosias Beneberu for his support and invaluable advice through the research.

I am thankful to my friends, family and all the staff at department of Civil Engineering, University of Texas.

July 20,2017

Abstract

HYDROCARBON POOL FIRE PERFORMANCE OF REINFORCED ELASTOMERIC BEARING PADS

Shashank Malal, MS

The University of Texas at Arlington, 2017

Supervising Professor: Nur Yazdani

Bearing pads are used as support for bridge girders to transfer the reaction forces to the substructure. They are designed to accommodate high axial loads from girder, shear deformations due to lateral thermal expansion of girder, and rotational deformation. Apart from these deformations bearing pads may also be subjected to thermal stresses due to daily temperature variations and extreme events like fire hazard. Current design methods do not account for these thermally induced stresses in elastomeric bearing pads.

The objective of this research is to study the hydrocarbon pool fire performance of elastomeric bearing pad. This research has three parts. The first phase involved hydrocarbon pool fire testing of a full-scale concrete bridge. Following the fire, hardness, shear modulus, compression set, and adhesion strength tests were conducted on the bearing pads as per the ASTM standards. In the second phase, the performance of bearing pads was studied by developing a thermo-mechanical analysis numerical model. Various performance parameters, such as shear strain, hydrostatic tensile strain, and bond stress were studied using linear and nonlinear material models for elastomer. In the third phase, a parametric study was conducted on different grades of bearing pad by exposing it to different temperatures and considering the effect of fillers.

All the properties of the bearing pads from the standardized tests with the exception of compression set remained within the limits. From numerical simulations, it is observed that nonlinear material behavior yielded much smaller shear strains at higher compressive loads when compared to linear elastic model and AASHTO (2014) results. From thermo-mechanical analysis, it was found that there will be significant thermal strains induced in elastomer when its temperature raises. However, it depends on many factors as magnitude of applied compressive stress, grade of elastomer and temperature. Increases of 74 %, 115 %, and 106 % in shear strain, hydrostatic tensile stress and bond stress, respectively, can be expected due to fire exposure for all grades of bearing pads, based on the level of applied compressive stress. Temperature has less contribution to shear strains beyond 50°C because of low thermal conductivity and high specific heat of elastomer, insulating interior parts of elastomer to external changes in temperature.

Table of Contents

List of Illustrations

List of Tables

Chapter 1

INTRODUCTION

1.1. Background

Elastomeric bridge bearings are in service for 60 years for thousands of bridges and similar structures around the world. Their first use was in Great Britain and they had a high demand during the World War II to use them as bearings for railway tracks and repairing the damaged bridges. "……breathtaking extension of the roads for cars after World War II a crucial factor for the development of bearings containing synthetic materials." (Wetzk 2017).

Initially bearings were simple objects such as steel blocks and wooden laths. But due to their limitations in simultaneously accommodating various deformations modes as compression, shear and rotation, there was a necessity to come up with new innovative solutions. Main objective was to accommodate high axial forces by having very high axial stiffness at the same time to be flexible in lateral direction to accommodate horizontal movements due to temperature changes and breaking force from the vehicle. Initially plain bearings were used and later rollers were added to accommodate horizontal movements. However, they had their short comings to accommodate rotation from the deflected shape especially when span length is significantly large to produce large rotational deformations in the end bearings. Different solutions and designs were developed in due course of time to address these issues. In today use, the American Association of State and Highway Transportation Officials (AASHTO 2014) recognizes different bearings types like plain elastomeric pad, fiberglass reinforced pad, pot bearing, and roller bearings and suggests the suitability of them in AASHTO LRFD Bridge Design Specifications (2014).

Steel reinforced elastomeric bearings are one of various bearing models made from synthetic materials like neoprene or from natural rubber. Their use had been extensive compared to other types mainly due to its simplicity of design, wide range of compressive and shear forces it can accommodate. It requires no maintenance and it is economical. Also, past research and field observations from the existing bearings have added more confidence in their future extensive usage (NCHRP 449 2001).

A steel reinforced bearing pad consists of layers of elastomer and mild steel which are vulcanized together to form a perfect bond. These bearings are available in different plan areas like square, rectangle, circular or other shapes. The elastomer is characterized by hardness and by varying it and the thickness, bearing can be designed to resist horizontal and vertical displacements.

Design of these elastomeric bearing pads, though simple and elegant, it offers a significant challenge for numerical simulations due to its nonlinear material property and near incompressibility. Though the elastomer is an elastic material, it has non-linear stress-strain behavior. Its material properties also depend on the factors such as shear strain, strain rate, specimen size, temperature, deformation history and boundary conditions. The nonlinear stress-strain curves, creep, hysteresis and other properties of elastomer are influenced not only by the method of fabrication but also by its previous history (Mullins, 1987). Typical stress-strain curves for rubber are highly nonlinear, hence it is not possible to assign a definite value to Young's modulus except in the region of small strain (Dorfmann 1999). Hence, the formula developed in their design used linear approximation of stress strain behavior, which is valid only in small strain range. Gent and Lindley (Gent and Lindley 1959a, Gent and Meinecke 1970, Lindley and Teo 1978) pioneered the analysis of laminated bearings and developed and presented a linearized analysis procedure. Conversy (1967) extended it to allow for finite values of the bulk

modulus, and Stanton and Lund (2004) provided numerical values of all the necessary coefficients, for different bulk modulus values (NCHRP 12-68 2006).

From designer's point of view, the unique properties of elastomers are – ability to undergo large strain and recover upon removal of load, being incompressible and the bulk modulus is many times larger than shear modulus, hence offering high axial stiffness and low shear stiffness. The stiffness of rubber especially in compression depend on the sample size, thickness and loaded area (Turner 1956). It is characterized by shape factor – which is ratio of loaded area to the area free to bulge. Higher shape factor implies higher stiffness.

Various researchers have studied the material behavior, performance related parameters of bearings but there has been no research on the fire performance of a bearing pad. Bridges are susceptible to fire due to the constant presence of vehicles and the potential for crashed or overturned vehicles to become fuel sources due to their flammable content. Vehicles involved in collision also cause a threat to bridge due to the combustion of their contents, including the onboard hydrocarbon fuel and, increasingly common, hybrid batteries (Quiel et al. 2015). Of all these, the most severe damage is caused when big trucks transporting large quantities of combustible cargo, hydrocarbon fuel or other flammable materials involve in a collision around the vicinity of the bridge (Beneberu, 2016). Apart from extreme events as fire hazard the bearing pads also experience the daily temperature variations which may induce thermal strains in elastomer. The present design codes do not account for these thermally induced strains in elastomer.

1.2 Objectives

There has been extensive research on individual material properties of elastomer and steel at high temperature (Yang et. al. 2014, Chen et al. 2006) but the

overall performance of bearing pads depends on various parameters such as – ‘confinement’ which affects the availability of oxygen during fire hazard, effect of pressure on the material properties on elastomer and steel, rate of heating and temperature history, bearing pad dimensions and exposed surface. So, current study is a first ever full-scale test conducted on the bearing pad in service to evaluate its performance at elevated temperature, specifically hydrocarbon pool fire.

The current research which focuses on hydrocarbon pool fire performance has three parts – Full scale testing, numerical simulations and parametric study. The full-scale testing consists of three bridge girders resting on bearing pads, subjected to hydrocarbon pool fire. One girder was wrapped with carbon fiber reinforced polymer (CFRP), another with CFRP and sprayed with fireproofing and third was a control girder without CFRP or fireproofing. Numerical simulations and thermo-mechanical analysis models are developed to study the various performance parameters of bearing pad under fire using nonlinear finite element software. A parametric study is conducted to account for parameters as change in thermal properties of elastomers due to the presence of fillers, different grades of elastomer and magnitude of temperature exposed to.

The present research was conducted with the following main objectives:

- Investigate the changes in material properties of bearing pad from the full-scale fire testing.
- To perform numerical simulations and evaluate its efficiency to predict various performance parameters under different material models for elastomer.
- To perform a thermo-mechanical analysis to find out the thermal strains produced in elastomer due to thermal expansion under heat.

- Perform a parametric study to consider the effect of elastomer grade, presence of fillers on thermal strains over different temperature ranges under different loading conditions.

1.3 Organization and Dissertation

Chapter 2 – Literature review

This chapter presents various relevant research on bearing pads, material properties, and design of bearing pad as per AASHTO.

Chapter 3 – Fire Test

Full scale testing done on bridge girders.

Chapter 4 – Material testing

Tested the material properties of bearing pad after the fire test and study its changes.

Chapter 5 – Numerical modelling

Modeled bearing pad and compare the results to the values obtained using AASHTO's provisions. Performed parametric study to consider the effect of fillers and different grades of elastomer.

Chapter 6 – Summary, conclusions and recommendations

The summary of research and conclusion drawn from test results and the numerical modelling are presented.

Chapter 2

LITERATURE REVIEW

2.1 High Temperature performance of bearing pad.

Bearing pads in service must accommodate various deformations due to live and dead loads from bridge girders, which induce shear strain in elastomer. The elastomer needs to be designed for these shear strains produced under different deformations. Apart from these mechanical shear strains, elastomer may also have thermally induced strains due to its temperature changes.

Temperature could be one of the most significant parameter which can induce shear stresses in elastomer due to differential thermal expansion between elastomer and steel. Elastomer has usually ten times more thermal expansion coefficient compared to metals (Bhowmick 2008). So, temperature can have significant induced thermal stresses along with mechanical stresses. But there has been no previous research on the thermo mechanical performance of bearing pads. Dorfmann et. al. (1999) had performed thermo-mechanical analysis of rubber-aluminum roll, in which heat was developed in elastomer due to cyclic loading where mechanical energy converts to heat energy. It was found out that there could be significant thermal strains produced in elastomer due to thermal expansion which needs to be accounted in its design.

Choi et. al. (2005) has studied the heat aging on vulcanized natural rubber. In which it is found that heat aging usually results in hardening of rubber as shown in Figure 2-1, which shows the nominal stress verses stretch ratio of elastomer heated for different time periods. Where nominal stress, also called as engineering stress was obtained by dividing force on the sample with the initial cross section area and stretch ratio was obtained by dividing original length by final length. In contrast, a temperature controlled

test at high temperature hardly changes the load-stretch curve as shown in Figure 2-2. Instead test at low temperature results in a high load-stretch ratio curve. Empirical equations were developed to predict the hardness of samples subjected to different temperature and aging time for elastomer specimens.

There has been research conducted on the high temperature effect on elastomer and steel, however there is no direct experimental testing or numerical simulations done on the whole bearing to study its fire performance. More details on the individual materials temperature performance will be discussed in detail in further sections.

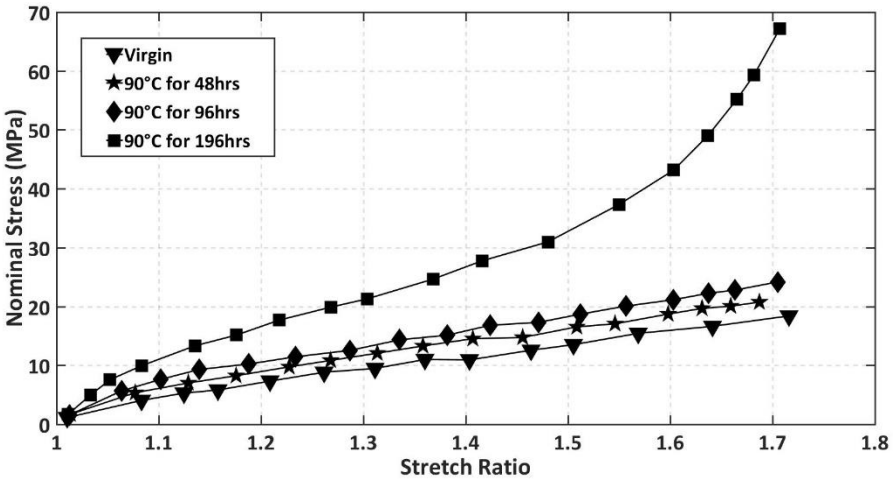

Figure 2-1 Load stretch ratio curves obtained from the tensile test for four differently aged specimens (Choi et. al. 2005)

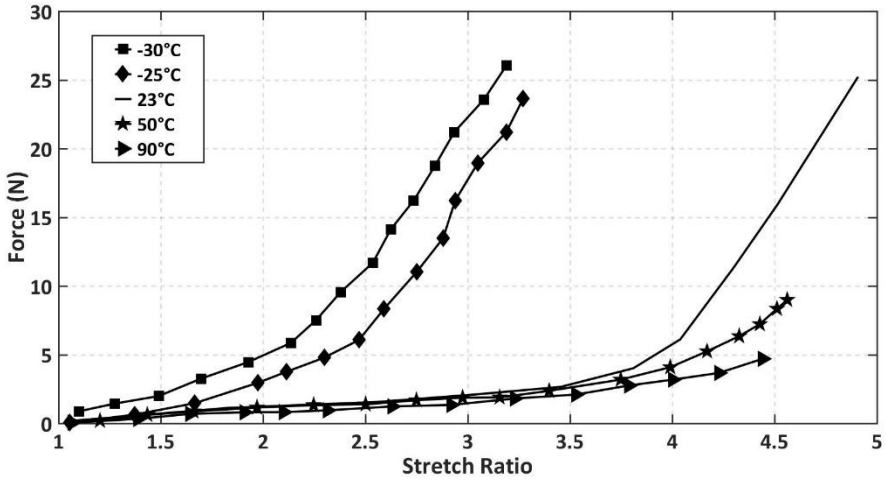

Figure 2-2 Load-stretch ratio curves obtained from the tensile test conducted in a temperature controlled chamber (Choi et. al. 2005)

2.2 Performance parameters of elastomeric bearing pad.

The effect of temperature on bearing pad can be studied using various parameters which applies to both strength and service limits. Based on the recommendation from the research of Alok (2000), which was based on the experience of several bearing manufactures, limits on different performance parameters were proposed for different elastomers in Table 2-1.

Here NR represents natural rubber and CR represents Neoprene. The number following it is the indicator for its hardness value.

Table 2-1 Performance Parameters of Bearing Pad

Dependent Variables	NR 50 (Natural Rubber)	CR 50 (Neoprene)
Max. Shear Strain	<6	<6
Max. Principal Strain	<2	<2
Triaxial tension (MPa)	<3.5	<3.53
Max bond stress (MPa)	<1.31	<1.81
Von Mises (MPa)	<345	<345

Here the performance parameters are based on strains rather than stresses. A single shear modulus is not sufficient to adequately represent the stress strain behavior of the elastomer, since it is dependent on the strain; hence evaluation criteria for rubber are based on strain rather than stress (Alok 2000). The aforementioned criteria according to Alok (2000) are explained in detailed below.

2.1.1 Maximum shear strain in elastomer

There are two types of shear strain in elastomer under combined axial and shear deformation: (a) direct shear strain due to shearing action (b) indirect shear strain due to bulging in lateral direction due to compressive force. Direct shear strain is limited to 1.75 (175%) whereas indirect shear strain is limited to 6 (600%). Total shear strain will be summation of direct and indirect shear strain. However direct shear strain is limited to only 0.5 by AASHTO (2014), so the limit suggested for total shear strain is 6 (600%).

The maximum shear strain equation given by AASHTO (2014) under pure compressive load is:

$$\gamma_a = D_a \frac{\sigma_s}{G\, S_i} \qquad \text{2-1}$$

In which for rectangular bearing:

D_a = 1.4

σ_s = average compressive stress due to total static or cyclic load from applied service load combinations (MPa).

G = Shear Modulus of elastomer (MPa).

S_i = Shape factor of interior layer of elastomer.

Shape factor is defined as ratio of loaded area to the bulging area on the sides of elastomer.

The above formulae for shear strain is developed based on following assumptions (NCHRP 12-68 2006)

- The rubber is perfectly bonded to the steel plates.
- The steel plates are rigid in axial compression.
- No edge cover exists.
- The rubber bulges laterally in a parabolic shape.
- Elastomer is assumed to be linear elastic material.

Determining shear strains in elastomer is complicated due to fact that elastomer is nearly incompressible, nonlinear, undergoes large deformations. Finite Element Analysis also pose significant short comings to determine shear strains due to formation of hourglass modes of distortions (NCHRP 12-68 2006). Hence linear approximation of material behavior was assumed in developing the equation.

2.1.2 Maximum Principal Strain in Elastomer

It is the maximum allowable uniaxial tensile strain in elastomer layers, which is limited to 2 (200%). This is because the AASHTO (2014) formulas are developed based on linear assumption of the elastomer behavior, which is valid only in small strain range (NCHRP 12-68 2006).

2.1.3 Tri-axial Tension in Elastomer

The maximum tri-axial tension is limited to three times the design shear modulus. Rubber is found to undergo internal cavitation at tri-axial tension beyond 3G, where G is the shear modulus (Gent and Tompkins 1969).

The intensity of hydrostatic tensile stresses increases with increase in applied compressive force. At $\sigma_a \approx 1.02\,GS$ the localized hydrostatic tension reaches the magnitude E, where σ_a is the compressive applied. When $\sigma_{hyd} \approx E \approx 3G$. Gent and Lindley (1959) observed that internal rupture of rubber begins. This internal rupture

failure of elastomer could be confused with debonding due to failure of adhesive bond as both initiates at the edge of steel shims. These hydrostatic tensile stresses cannot be predicted by the linear theory; however, they are directly related to the shear strain in elastomer. Hence AASHTO (2014) in method A – Design of bearing pads, this is addressed by limiting the applied compressive stress to be less than 1.02GS.

2.1.4 Maximum Bond Stress

This bond stress is developed at steel and elastomer interface, resulted from the tensile stress and shear stress developed at interface due to external loads. It is limited to stress corresponding to shear strain of 2 (200%) from simple shear test on elastomer.

2.1.5 Maximum von Mises Stress in Steel Laminates

This represents the stress in steel laminates corresponding to von Mises failure criteria. In this theory failure occurs when distortional energy per unit volume equals to the yield stress in simple tension test.

$$(\sigma_1 - \sigma_2)^2 + (\sigma_2 - \sigma_3)^2 + (\sigma_3 - \sigma_1)^2 = 2\sigma_{yp}^2 \qquad 2\text{-}2$$

σ_1, σ_2, σ_3 are the principal stresses and σ_{yp} is the yield strength of the material. The von Mises calculated by the finite element analysis is:

$$\sigma = \sqrt{\frac{(\sigma_1 - \sigma_2)^2 + (\sigma_2 - \sigma_3)^2 + (\sigma_3 - \sigma_1)^2}{2}} \qquad 2\text{-}3$$

2.3 Axial Stiffness

It is the ratio of the axial load to axial deflection at 3.8Mpa (550psi). Axial stiffness is directly proportional to the vertical deflection. For the bridge girders if there is excessive axial deflection it results in uneven settlement and can result in excessive stress in the girders.

Stanton and Lund (2004) expressed bearing stiffness in terms of shape factor, S as

$$K_a = \frac{P}{\Delta_a} = \frac{EA(A_a + B_a S^2)}{t} \quad \text{2-4}$$

S = shape factor

A_a, B_a = dimensionless constants, which must be computed from the experimental or numerical models.

Δ_a = axial displacement

t = thickness of elastomer

2.4 Shear Stiffness

It is the ratio of shear force to the shear deformation at shear strain corresponding to 0.5. Since bridge girder expands and contracts under temperature differences, its horizontal movements need to be accommodated by the bearing. AASHTO (2014) has proposed using shear modulus of elastomer as shear modulus of bearing pad. Hence the shear strain is calculated as

$$\gamma_s = \frac{\Delta_s}{h_{rt}} \quad \text{2-5}$$

Δ_s – max. shear deformation

h_{rt} – total thickness of elastomer

2.5 Rotational Stiffness

Rotational stiffness represents the ratio of cocking moment to the cocking rotation corresponding to 1° rotation of bearing. However rotational stiffness of elastomeric bearing pad is not very important because if there is a significant rotation it is recommended to use cylindrical or spherical bearing.

Stanton and Lund (2004) has proposed rotational stiffness in terms of shape factor as

$$K_r = \frac{M}{\theta_L} = \frac{EI}{t}(A_r + B_r S^2) \quad \text{2-6}$$

A_r and B_r are dimensionless constants, which must be computed from the experimental or numerical models.

θ_L = Rotation angle applied to each layer of the bearing

S = Shape factor = ratio of loaded area to the bulging area on the sides

t = thickness of elastomer

2.6 Standard specifications

In the United States, all the steel reinforced bearing pads for bridge girder support must adhere to the specification of AASHTO M251 (2011) and designed as per latest version of AASHTO LRFD Bridge Design Specifications. These standards are discussed in brief below.

2.6.1. AASHTO M251

Standard Specifications for plain and laminated elastomeric bridge bearings, M251-06(2011)

This specification covers requirements for material property of elastomers for both plain and laminated. Bearings designed under this specification shall adequately satisfy for thermal expansion & contraction, rotation, camber changes, creep and shrinkage.

Elastomers accepted are

-Virgin crystallization resistant poly-chloroprene (neoprene)

- Virgin natural poly-isoprene (natural rubber)

Elastomers are classified into different grades based on temperature zone in which they are used – 0, 2, 3, 4, 5. It is because at lower temperature, the shear modulus increases and hence the bearing pad stiffens, this could lead to the increased force onto the substructure. So, by using different grades the shear stiffness could be controlled at required temperature zones. It also discusses about various tests for shear, creep,

compressive strain and about design tolerances. Table 2-2 shows the minimum material property requirement for elastomers and Table 2-3 shows the optional material tests on bearing pads.

Table 2-2 Minimum material property requirements for elastomers

Material property	ASTM Std.	Test requirements	Polyisoprene (Natural Rubber – NR)	Polychloroprene (Neoprene)	Units
Physical properties	D412	Min Shear modulus	0.55(79.7707)	0.55(79.7707)	MPa(psi)
		Min. tensile strength	15.5(2248.085)	15.5(2248.085)	MPa(psi)
		Min. Ult. Elongation	450	400	%
Low temperature brittleness	D746 Procedure B	Grade 0 and 2 – No test required	-	-	
		Grade 3 – Test at -40°C (-40°F)	Passes	Passes	
		Grade 4 – Test at -48°C (-54.4°F)	Passes	Passes	
		Grade 5 – Test at -57°C (-70.6°F)	Passes	Passes	

Table 2-3 Optional material tests for bearing pads

Material Property	ASTM Standard	Test requirements	NR			CR			Units
			50	60	70	50	60	70	
Physical properties	D 2240	Hardness	50±5	60±5	70±5	50±5	60±5	70±5	Shore A
	D 412	Min. tensile strength	15.5 (2248)	15.5 (2248)	15.5 (2248)	15.5 (2248)	15.5 (2248)	15.5 (2248)	MPa (psi)
		Min. ult. Elongation	450	400	300	400	350	300	Percent
Heat resistance	D 573 at Specific temp.	Specific Temperature of the test	70 [158]	70 [158]	70 [158]	100 [212]	100 [212]	100 [212]	C (F)
		Aging time	168	168	168	70	70	70	Hours
		Max. change in durometer hardness	10	10	10	15	15	15	Shore A
		Max. change in tensile strength	-25	-25	-25	-15	-15	-15	Percent
		Max. change in ult. Elongation	-25	-25	-25	-40	-40	-40	Percent
Compression set	D 395 Method B at specific temp	Specific Temperature of the test	70 [158]	70 [158]	70 [158]	100 [212]	100 [212]	100 [212]	°C (F)
		Max. permissible change (after 22hr)	25	25	25	35	35	35	Percent
Low temp. brittleness	D 746 Procedure B	Grade 0 and 2 –No test required							
		Grade 3 – Test at -40 C (-40F)	pass	pass	pass	pass	pass	pass	
		Grade 4 – Test at -48 C (-54.4F)	pass	pass	pass	pass	pass	pass	
		Grade 5 – Test at -57 C (-70.6F)	pass	pass	pass	pass	pass	pass	

2.6.2 AASHTO LRFD – Bridge Design Specifications –

Elastomeric bearing pads designed as per AASHTO (2014) has two design methods give in Chapter 14. They are: Method-A and Method-B. Design method Method-A yields low capacity for bearing pads compared to design Method B. But to make advantage of increased bearing capacity using Method B, additional testing and quality control is required. These design methods are explained in brief below.

2.6.2.1. AASHTO design requirements – Method B

This is the latest design method included in AASHTO (2014). The most important parameter to limit in bearing pad is shear strain. Elastomer is almost incompressible, so when a compressive load is applied, elastomer due to poisons effect bulges out. This bulging action is resisted by steel plates and hence creates large shear strains at the interfaces causing de-bonding which is the most common failure.

Method-B directly addresses these shear strains by estimating their numerical value under compression, shear, rotational deformations and sets a limit for combined shear strain. This allows a more versatile design options. The Figure 2-3 shows the deflected shapes and location of maximum shear strain in elastomers under different loading conditions.

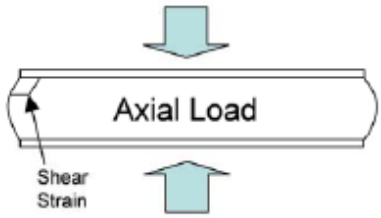

(a) Compression

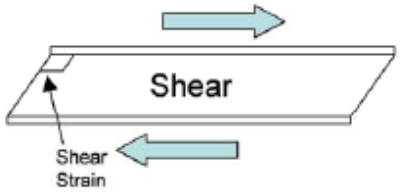

(b) Shear

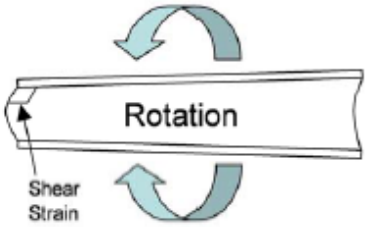

(c) Rotation

Figure 2-3 Deformation of laminated elastomer layer under different deformations (NCHRP 12-68 2006)

AASHTO (2014) method B directly addresses the shear strains generated under different loading conditions and limits them as shown below.

$$(\gamma_{a,st} + \gamma_{r,st} + \gamma_{s,st}) + 1.75(\gamma_{a,cy} + \gamma_{r,cy} + \gamma_{s,cy}) \leq 5 \qquad 2\text{-}7$$

γ – Shear strain

a-axial s-shear r-rotation st-static load cy-cyclic load

also $\gamma_{a,st} \leq 3.0$

Each layer of elastomer is characterized by it shape factor. Shape factor of a layer of an elastomeric bearing is given by –

(For rectangular shape)

$$S_i = \frac{L\,W}{2h_{ri}(L+W)} \qquad 2\text{-}8$$

L = plan dimension of the bearing perpendicular to the axis of rotation under consideration

W = plan dimension of the bearing parallel to the axis of rotation under consideration

h_{ri} = thickness of the interior elastomer layer

The following equations are given by AASHTO (2014) to calculate the shear strains under different loading conditions.

Shear strain due to axial load –

$$\gamma_a = D_a \frac{\sigma_s}{G\, S_i} \qquad \text{2-9}$$

D_a = 1.4 for rectangular bearing

= 1 for circular

σ_s = applied stress (MPa)

G = Shear Modulus (MPa)

S = Shape Factor

Shear strain due to rotation –

$$\gamma_r = D_r \left(\frac{L}{h_{ri}}\right)^2 \frac{\theta_s}{n} \qquad \text{2-10}$$

D_r = 0.5 for rectangular bearing

n = number of internal layers

h_{ri} = thickness of i^{th} layer of elastomer

θ_s = rotation angle

L = length of bearing pad along the rotation

Shear strain due to shear deformation –

$$\gamma_s = \frac{\Delta_s}{h_{rt}} \qquad \text{2-11}$$

Maximum shear deformation (horizontal movement) at service is limited to 50%

i.e.,

$$h_{rt} \geq 2\Delta_s \quad \text{2-12}$$

h_{rt} = total elastomer thickness

Δ_S = max. shear deformation from applicable service load.

In bearings with externally bonded plates at top and bottom, the peak hydrostatic stress shall satisfy

$$\sigma_{hyd} \leq 2.25G \quad \text{2-13}$$

$$\sigma_{hyd} = 3GS_i^3 \frac{\theta_s}{n} C_\alpha \quad \text{2-14}$$

$$C_\alpha = \frac{4}{3}\left[\left(\alpha^2 + \frac{1}{3}\right)^{1.5} - \alpha(1 - \alpha^2)\right] \quad \text{2-15}$$

$$\alpha = \frac{\varepsilon_a}{S_i}\frac{n}{\theta_s} \quad \text{2-16}$$

$$\varepsilon_a = \frac{\sigma_s}{3\, B_a G S_i^2} \quad \text{2-17}$$

for rectangular bearings: Ba = 1.6

ε_a = average axial strain

There would be tri-axial tensile stresses developed in the center of bearing pad under rotation. These stresses can produce tensile failure in elastomer. Hence, AASHTO (2014) limits these stresses by limiting the applied rotation by equation 2-14 mentioned above.

Compressive deflections are limited so that there won't be damage to the supporting structural elements of bridge. In absence of test data following equation 2-18 or design charts shown in Figure 2-4 and Figure 2-5 can be used to calculate instantaneous deflection.

$$\varepsilon = \frac{\sigma}{(4.8GS^2)} \qquad \text{2-18}$$

AASHTO (2014) specifies the minimum elastomer grade for each temperature zone to account for the shear stiffening of elastomer at low temperatures. Beginning from 0°F and below 45°F 50-year low temperature, the various low temperature elastomer grades as classified as Grade – 0,2,3,5.

2.6.2.2. AASHTO design requirements – Method A

In method A unlike method B, shear strains in elastomer are limited by limiting the average compressive stress applied.

Compressive stress at service ≤ $1.25GS_i$

≤ 1.25 ksi

These limits are adjusted so that the maximum hydrostatic tensile stress in elastomer under compression is less than 3G.

The shear deformation is limited by shear strain to be less than 50%. Hence the total elastomer thickness must be greater than twice the expected lateral displacement of bearing pad under shear deformation.

Compressive deflection shall be calculated by using Figure 2-4 and Figure 2-5.

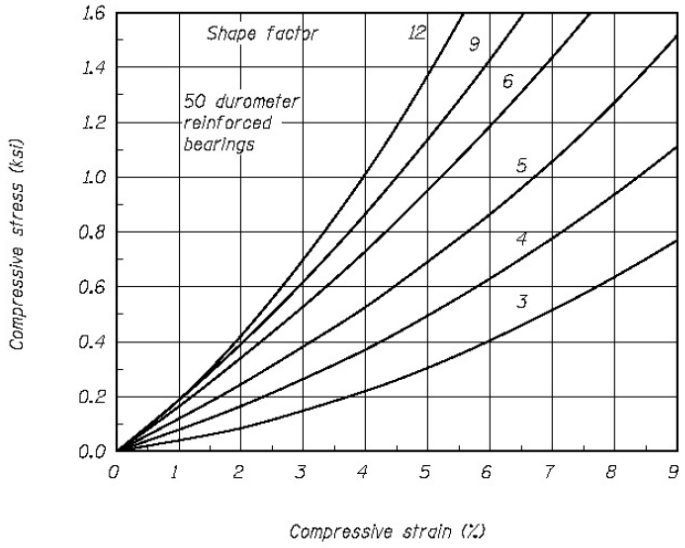

Figure 2-4 Stress-Strain plot for 50 grade elastomer layers (AASHTO 2014)

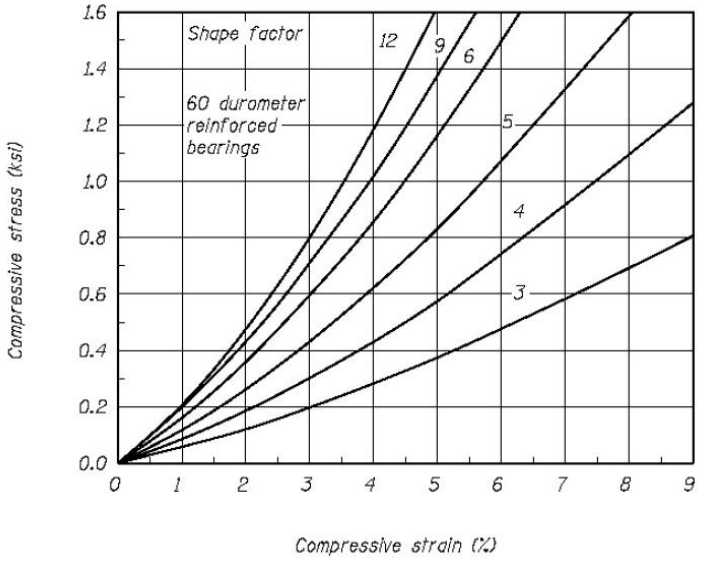

Figure 2-5 Stress-Strain plot for 60 grade elastomer layers (AASHTO 2014)

In Method A design – rotation and compression are controlled by limiting the applied compressive stresses whereas in Method B it is achieved by limiting strains.

Method A is not economical and yields low capacity and makes design more challenging with combination of loads.

2.7 Effect of bearing pads on design of concrete bridges

The bearing pad – bridge beam interface defines the support boundary conditions which may affect the performance of the bridge. Yazdani et al. (2000) studied this effect by varying the stiffness values of bearing pad in the finite element models of AASHTO Type III and IV beams, subjected to simulated static truckloads. The results from numerical models were compared with the field tests. It was concluded that, in general the restraining effects of bearing pads, due to various reasons as creep, temperature, aging is beneficial to the performance of beams and the bridge. By increasing the shear modulus, the maximum deflection and tensile strains were appreciably reduced.

AASHTO (2014) standard specifications limits the horizontal forces imparted to the substructure be limited to 5%. Yazdani et al. (2000) has observed that, unless there is a drastic increase in shear modulus as about 50 times, the imparted horizontal forces onto substructure are well below 5%.

Hence the increase in shear modulus of elastomer due to heating can be beneficial to the performance of bearing pad, provided its value is less than 0.175 ksi as limited by AASHTO (2014) to avoid the brittle failure.

2.8 Elastomer properties

2.8.1 Mechanical Properties

Elastomer is a nonlinear elastic, incompressible material. So, it can be defined by strain energy density function proposed by various researchers. The strain energy density used in current research was introduced by Yeoh (1991).

Yeoh model is given as:

$$W = C_{10}(I_1 - 3) + C_{20}(I_1 - 3)^2 + C_{30}(I_1 - 3)^3 \quad \text{2-19}$$

W – Strain energy density function

I_1, I_2, I_3 are the strain invariants

C10, C20, C30 are material constants shown in Table 2-4. These values are directly taken from NCHRP 12-68 (2006). These material constants are obtained by performing a regression analysis of experimental data in simple shear test and adjusted such that it produces a secant modulus of 0.68 MPa (100psi) at 50% shear strain in simple shear test.

Table 2-4 Hyper-elastic material constants for elastomer

C10	C20	C30
344.47 KPa	-6.216 KPa	0.292 KPa

Elastomer can be approximated to be a linear model in small strain range. All the formulas mentioned in AASHTO (2014) to find the shear strains also assumed linear behavior. Hence for linear elastic approximation, the data given by the manufacturer (COSMEC INC.) is shown in Table 2-5.

Table 2-5 Linear elastic material constants for elastomer

Shore Hardness	50
Young's Modulus	2.2 Mpa (312psi)
Shear Modulus	0.68 Mpa (100psi)
Poisson's Ratio	0.499
Density	1.24 Mg/m3

2.8.3 Elastomer properties at elevated temperature

Elastomer properties changes based on the temperature (Alok 2000). The change could be temporary or permanent based on the magnitude of temperature and its frequency of occurrence.

Tobolsky (1960) conducted experiments on rubber strips, which are subjected to a uniaxial stretch and held at a fixed higher temperature for some time interval and then brought back to the initial temperature. It is observed that at temperatures above T_{cr}, (say 100^{o}C), called the chemorheological temperature, there is reduction in tensile stress and a permanent set(stretch) is induced. From the data analyzed, the researcher developed a relation between Cauchy stress tensor $\sigma(t)$ and uniaxial stretch ratio λ assuming neo-Hookean behavior as

$$\sigma(t) = 2n(t)kT\left(\lambda^2 - \frac{1}{\lambda}\right) \qquad 2\text{-}20$$

T is the absolute temperature, k is the Boltzman constant and n(t) is the current crosslink density. Decrease in tensile stress $\sigma(t)$ is attributed to the scission of molecular network crosslinks which decreases crosslink density n(t) and permanent stretch is attribute the formation of new crosslinks in stretched state(healing). Alan Wineman (2003) developed a comprehensive thermos-mechanical model which is beyond the

scope of this research, to account for the microstructure change in elastomer. It was concluded that in natural vulcanized rubber there is substantial stress relaxation at elevated temperatures, material softening, permanent set and creep due to microstructure changes.

Polymer form also depends on temperature. As temperature increases it changes from glassy to rubbery form at glass transition temperature and from rubbery to melt at melting temperature as shown in Figure 2-6. In glassy form, it behaves like solid and hard, in rubbery region it is soft, flexible and elastic and in melt form it behaves as liquid.

Tg is called glass transition temperature which applies to all polymers (amorphous, crystalline, rubbers, thermosets, fibers etc.). It is defined as temperature wherein a significant loss of modulus occurs.

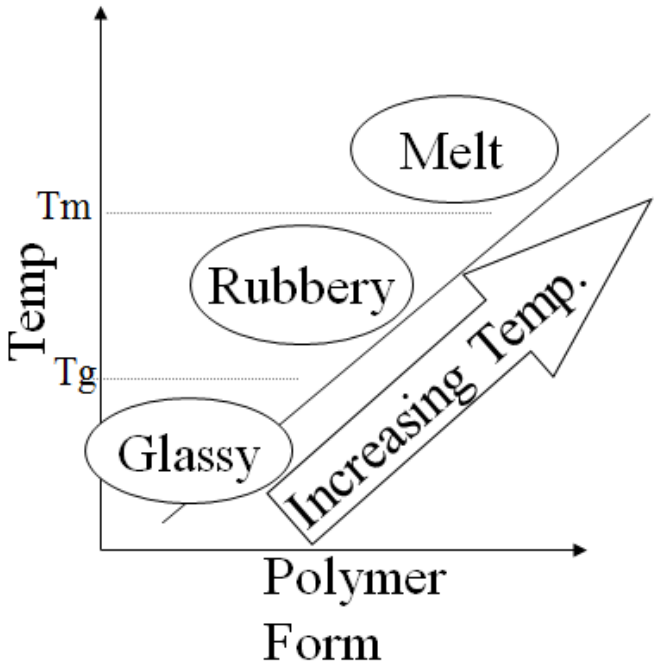

Figure 2-6 Polymer forms at different temperatures

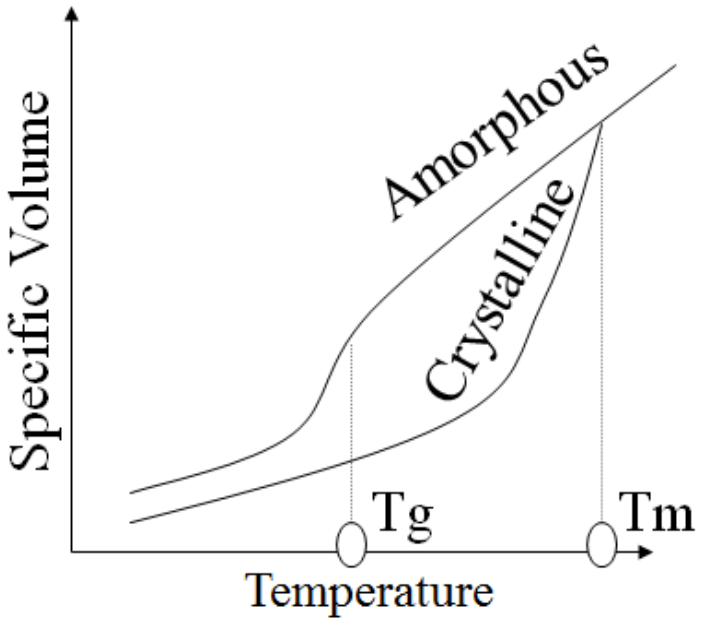

Figure 2-7 Amorphous and crystalline polymers

The glass transition temperature for neoprene is around -42°C (George et. al 1990). The maximum working temperature suggested for neoprene and natural rubber is 100°C (J.J.Short Ass.). In absence of oxygen most types of rubber can survive up to 175°C (Brown,1996). At this temperature, there is degradation of elastomer and loss of physical properties. The presence of oxygen is also important factor in determining the resistance of rubber to elevated temperatures.

Alok (2000) conducted experiments to find the variation of shear modulus with temperature for 50 durometer elastomer and its results are shown in Figure 2-8.

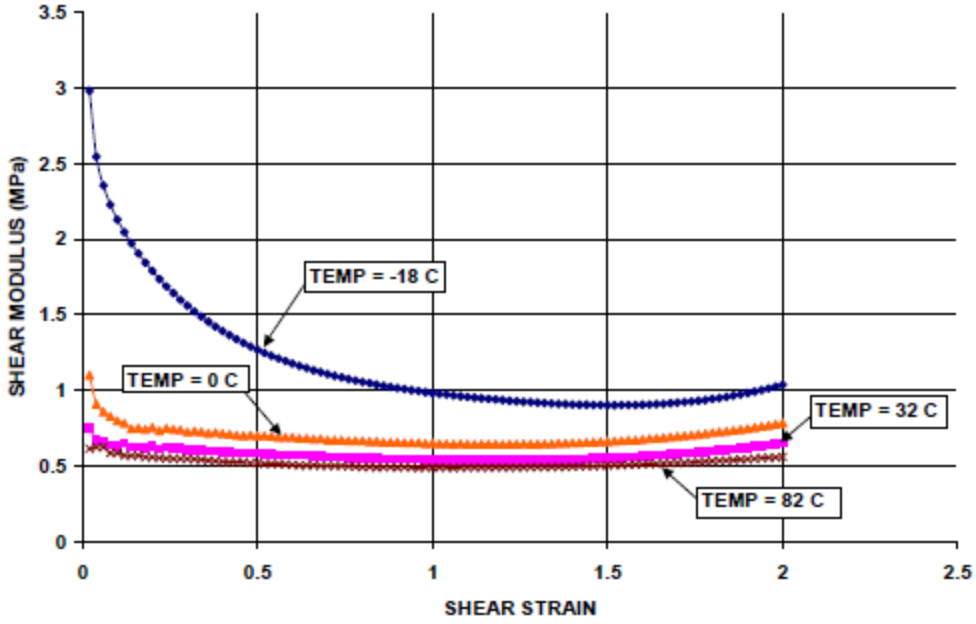

Figure 2-8 Shear Modulus of NR50 at various temperatures (Alok 2000)

It can be observed that shear modulus changes are not predominant at higher temperatures compared to lower temperatures. Author also performed accelerated aging test by heating samples of different sizes and noting the percentage change in shear modulus, which is the most important property which is of primary importance. From the previous filed observations from various bridge sites it is found that elastomer is very much resistant to aging effects. Most of the degradation is occurred only in the exposed cover and damage didn't penetrate inside the elastomer as the oxidized elastomer acts as shield in further degradation of elastomer. Alok (2000) performed experiments on various sample sizes and concluded that aging doesn't affect the performance of bearing pad as the size of the bearing pad is significantly large compared to the test sample and it takes hundreds of years even for a sample of size 3 in. X 3 in. specimen to change its shear stiffness by 10 percent.

A similar research performed by Choi (2005), developed empirical equations to determine the hardness of sample exposed to fire load after cooling down for different temperature and time.

$$K1 = LOG(T/23)^{2.958} \quad (2\text{-}21)$$

$$K2 = (T/477.2)^{0.5263} \quad (2\text{-}22)$$

$$IHRD = 62*EXP(K1*K2) \quad (2\text{-}23)$$

K1 and K2 are the parameters that account for the effect of temperature and period respectively.

T is the heat aging temperature in degree Celsius

t – time of aging in hours

62 is the initial hardness of the elastomer.

However, this equation will depend on the sample size, material property of elastomer etc., so the equations above may have to be recalibrated to use it for other specimens. Also, some of the observations made are –

- Samples aged at higher temperatures are stiffer after cooling than that of at low temperatures.
- Samples aged for more time are stiffer after cooling than that at lower times.
- Samples on which when temperature controlled tension test was performed, higher temperatures had no significant effect on the slope which is modulus of elasticity, but however the samples at lower temperatures like -15^0C showed a significant stiffening.
- Samples tested after cooling for a certain time did not show any change in molecular structure and property remained same when brought back to normal room temperature unlike aging at high temperatures.

Hence the elastomer property changes with temperature depends on factors as the magnitude of temperature, time, sample size and the stress relaxation. This makes the study of bearing pad with temperature more challenging. Because it is observed that there is no significant change in elastic modulus in temperature controlled stress strain curves and no significant damage due to aging in elastomer, the mechanical properties of elastomer are assumed to remain constant with temperature in this research. Though there is hardening in elastomer due to temperature, it mostly occurred in the exterior parts as it depends on sample size as observed from experiments of Alok (2000). Considering the size of bearing pad, the contribution of exterior cover hardness to the performance of entire bearing pad could be neglected. The most important mechanical property which induces thermal strains in bearing pad is its coefficient of thermal expansion. Elastomer has very high thermal expansion coefficient compared to steel. So there could be significant thermal strains due to differential expansion of steel and elastomer.

Thermal conductivity of elastomer is 0.2 W/m K (ASDTR61-234) and variation of its specific heat with temperature is shown in Figure 2-9 . Elastomer is a poor conductor of heat compared to steel and the variation of its thermal conductivity with temperature is negligible. The specific heat with temperature is shown below, the sharp fall in specific heat after 200°C is due to degradation (Mandal et. al. 2014).

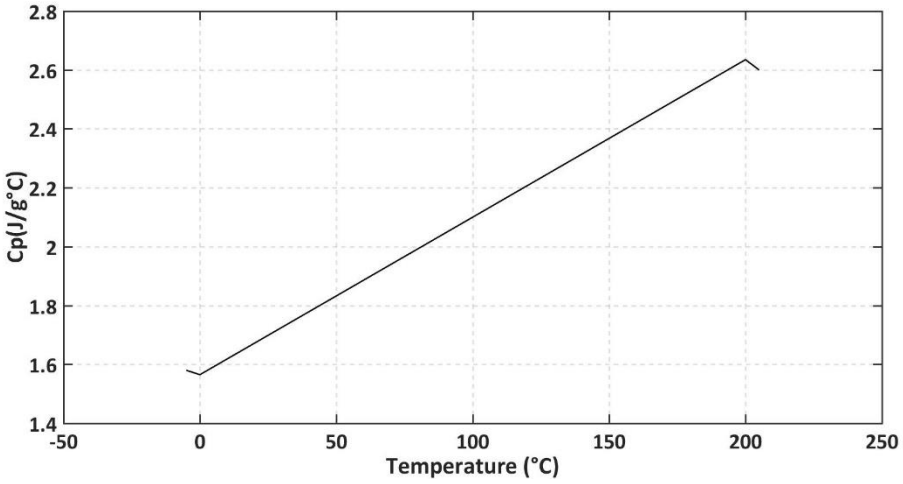

Figure 2-9 Variation of specific heat of elastomer with temperature

2.8.3.1 Effect of fillers in elastomer

The thermal properties mentioned above for elastomer are taken for a pure sample which doesn't have any fillers added to it. But fillers may change the thermal properties of elastomer.

Fillers are fine crystalline particles which are widely used in elastomer for various applications. They are small hard particles usually of carbon or inorganic origin. These fillers act as reinforcing agents to improve the material properties of elastomer as abrasion resistance, tensile strength, hardness. The size, shape and surface activity determines their reinforcing ability.

The main focus of the parametric study in this research was to account for the change in the thermal properties of elastomer due to the presence of fillers. In rubber compounds the main reinforcing fillers used are silica and carbon black. It is used in varied proportions by different manufactures to achieve different desired material properties. Usually a filler concentration of 25 phr (parts per hundred rubber) which

includes silica, carbon black and any others depending on the manufacturers patents is used.

Mandal et. al. (2014) has conducted research on variations in specific heat of natural rubber filled with different fillers and concentrations. It was found that specific heat of elastomer increases with the presence of fillers. This is because the free volume in rubber decreases and molecular weight increases in terms of cross-linking. This reduces the segmental motion of molecules and increases specific heat. Among various fillers considered the nanosilica was the most active filler.

Oggermuller (2008) has conducted studies on the effect of fillers on the thermal conductivity of elastomers. By adding carbon black up to 100 phr the maximum value in thermal conductivity was found to be 0.45 W/mK compared to 0.22 W/mK without adding any filler.

2.9 Steel laminates

2.9.1 Mechanical properties of steel

As per AASHTO M251 (2011) the steel laminates used shall be from rolled mild steel conforming to ASTM A 36/A 36M, ASTM A 1011M, or equivalent, unless otherwise specified by the purchaser. The laminates shall be of the thickness specified by the purchaser and have a minimum nominal thickness of 1.52mm (0.0598 in.) Holes in laminate are not allowed as it causes stress concentrations. Table 2-6 shows the mechanical properties of A570 steel.

Table 2-6 Mechanical properties of steel

Grade	ASTM A570 OR A1011
Modulus of Elasticity	200Gpa
Poisson's ratio	0.3
density	7.8 Mg/m3
Yield Stress	235 Mpa

2.9.2 Steel properties at elevated temperature

The material properties of steel like elastic modulus, yield strength depends on the temperature. Figure 2-10 shows the temperature dependent stress strain curves of steel. It is observed from these figures that strength and stiffness both drops with temperature.

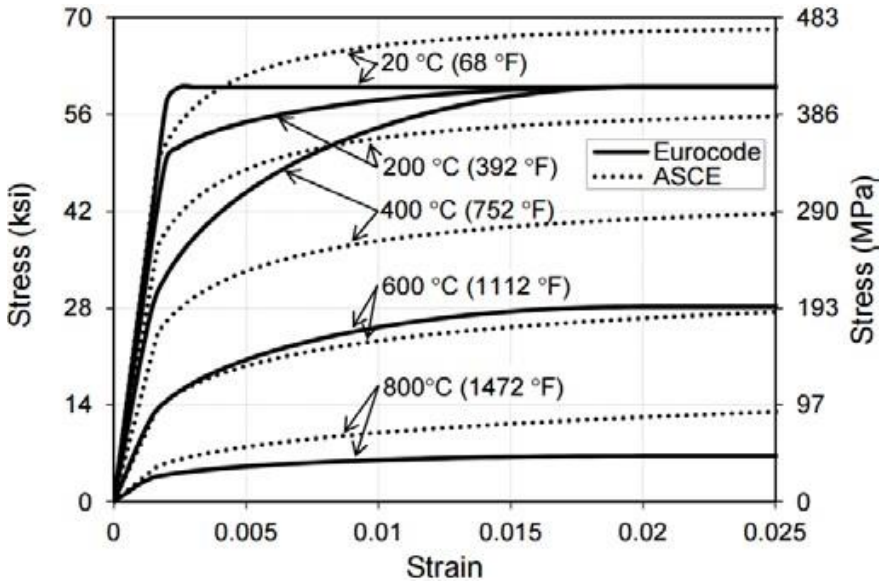

Figure 2-10 Stress Vs Strain for mild steel at different temperatures (Eurocode 3, 2005)

Figure 2-11 and Figure 2-12 shows the variation of thermal conductivity and specific heat of mild steel with temperature. Thermal conductivity linearly decreases up to

800°C and then remains constant. Specific heat of steel shows a gradual change with a spike at 735°C due to crystal phase change of steel (Wang et al. 2013).

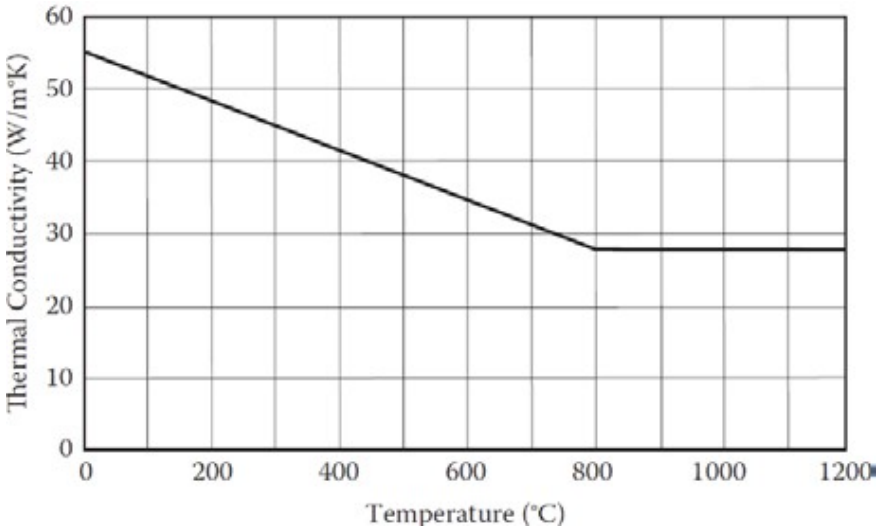

Figure 2-11 Thermal Conductivity of steel Vs Temperature (Eurocode 3, 2005)

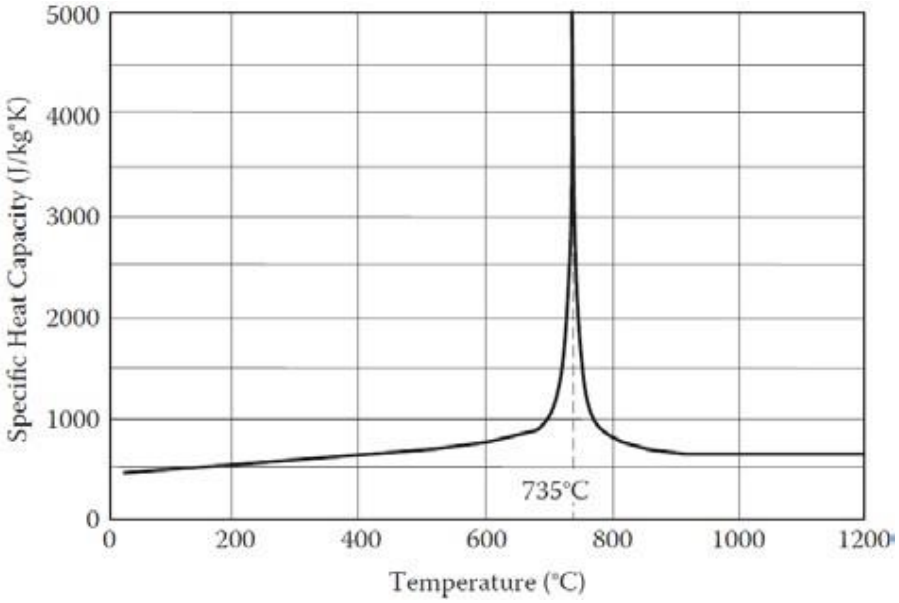

Figure 2-12 Variation of specific heat of steel with temperature (Eurocode 3, 2005)

Chapter 3

FIRE TEST

The fire test mentioned here is part of the research conducted by Beneberu (2016). The main objective of that research was to study the effect of fire on bridges in general and FRP strengthened girders specifically. The scope of present research is to study the effect of fire on performance of bearing pads on which those girders were placed.

3.1 Experiment Setup

The Fire test was performed on a full-scale concrete bridge comprised of three Texas Standard TX28 girders, each spanning 10.1 m (33 ft.) and spaced at 1.82 m (6ft.) on center. All girder ends are supported on bearing pads. A deck is supported on the girders whose dimensions are – 9.754 m (32ft.) long, 5.486 m (18 ft.) wide, 0.914 m (3ft.) overhang and 20.32 cm (8 in.) thickness. The girders were designed for self-weight, dead load from the deck, and AASHTO (2014) HL-93 live load. The arrangement of girders and slab is shown in Figure 3-1.Girder spacing and reinforcement details are shown in Figure 3-2.

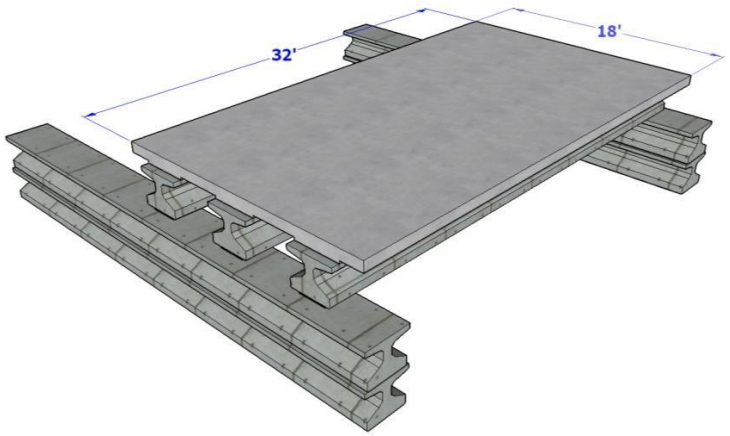

Figure 3-1 Girder Arrangement (Beneberu 2016)

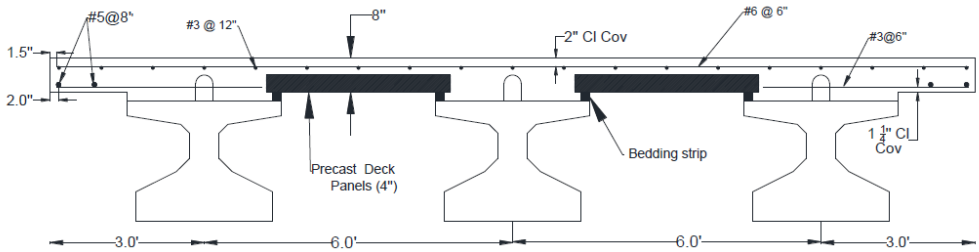

Figure 3-2 Deck Reinforcement and Girder Spacing (Beneberu, 2016)

The deck was loaded with zipper barriers as shown in

Figure 3-3 to simulate the vehicular live load.

Figure 3-3 Simulated AASHTO live load (Beneberu, 2016)

Four thermocouples were placed on the bearing pads as shown in Figure 3-4. T-1, T-2, T-4 are placed facing inside and T-3 was placing facing away from fuel pan as shown. Figure 3-5 shows the thermocouple T-3 arranged on the bearing pad.

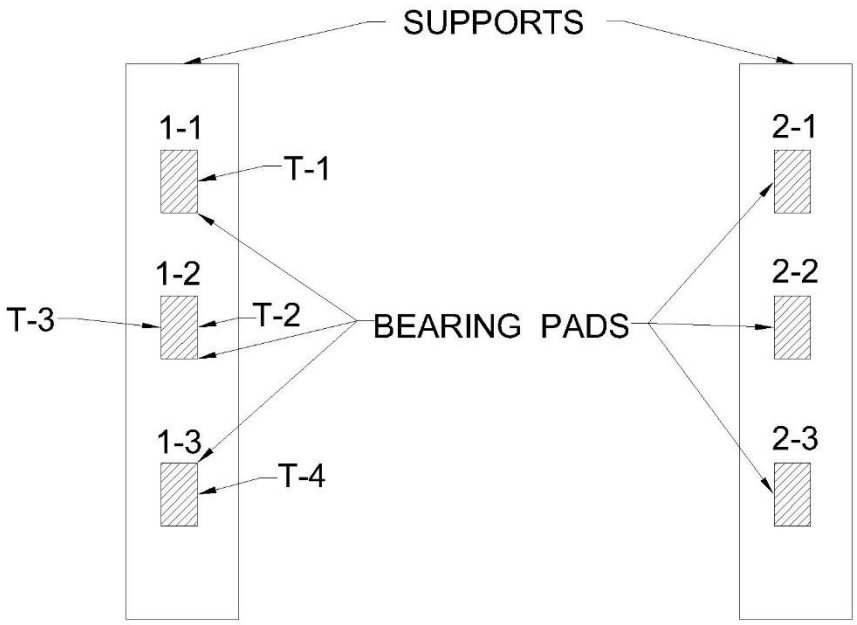

Figure 3-4 Thermocouple and bearing pad placement

Figure 3-5 Thermocouple on bearing pad

To ensure uniform heating, the fire test was scheduled on a day where there will be non/minimal wind. On the scheduled day, the pan was filled with water up to 0.254 m (10'') depth followed by E-III fuel. The fire was set on and the temperature continued for an hour before it decreased as shown in Figure 3-6. Though it was calm and non-windy at the beginning of the test, but after few minutes a south-east wind came and disturbed the even distribution of fire. The wind persisted till the end of the test. The test was conducted for one hour by burning 4.23m^3 (1140 gallons) of E-III fuel.

Figure 3-6 Fire Test (Beneberu, 2016)

3.2 Results and Discussion

Figure 3-7 shows the bearing pad after fire test. As it can be observed from

Figure 3-8, the temperature from the fire reached as high as 1131°C at the mid-span of the bridge before it decreased. The temperature from thermocouple attached to bearing pads are shown form Figure 3-9 to Figure 3-11.

Figure 3-7 Bearing pad after fire test

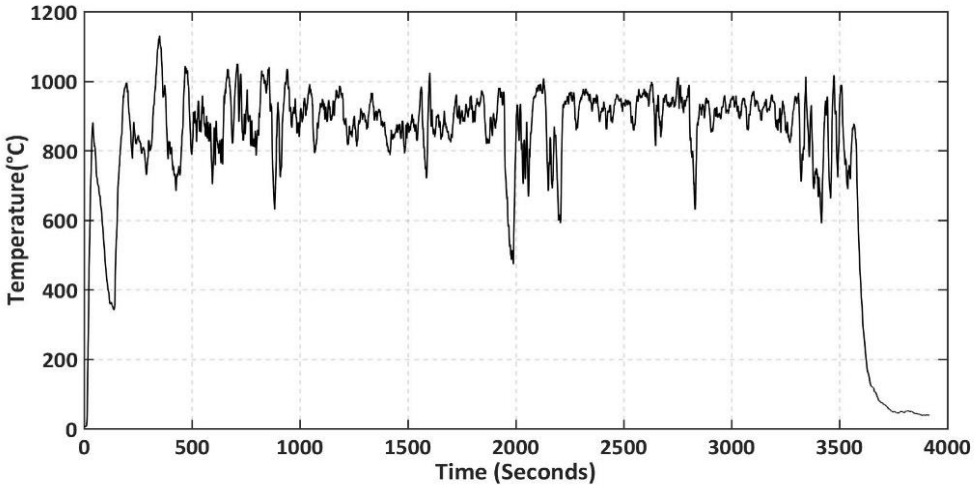

Figure 3-8 Fire temperature versus time curve (Beneberu, 2016)

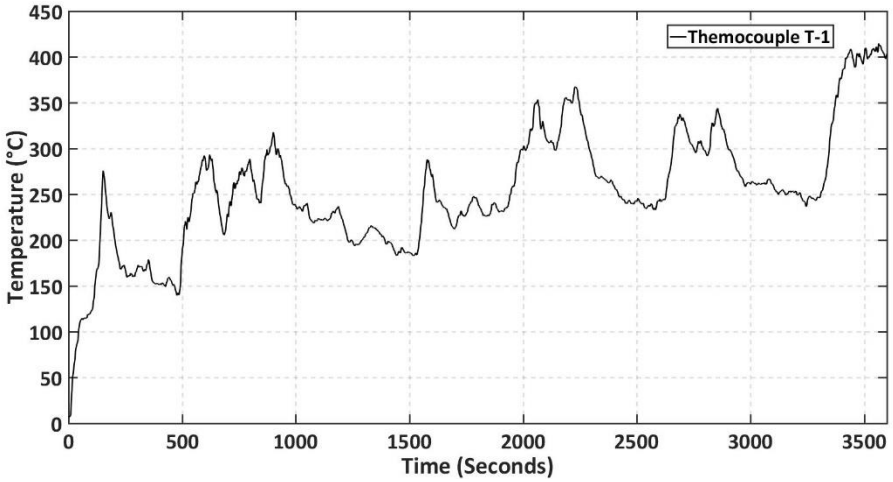

Figure 3-9 Thermocouple reading from T1

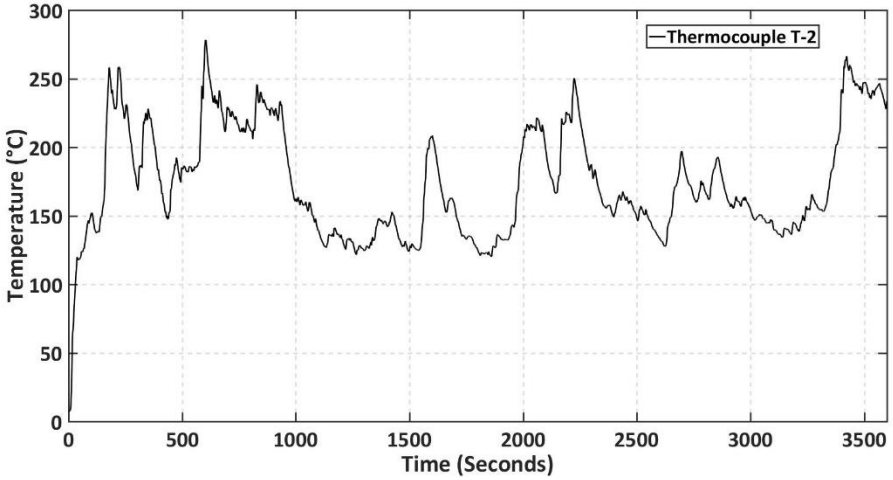

Figure 3-10 Thermocouple reading from T2

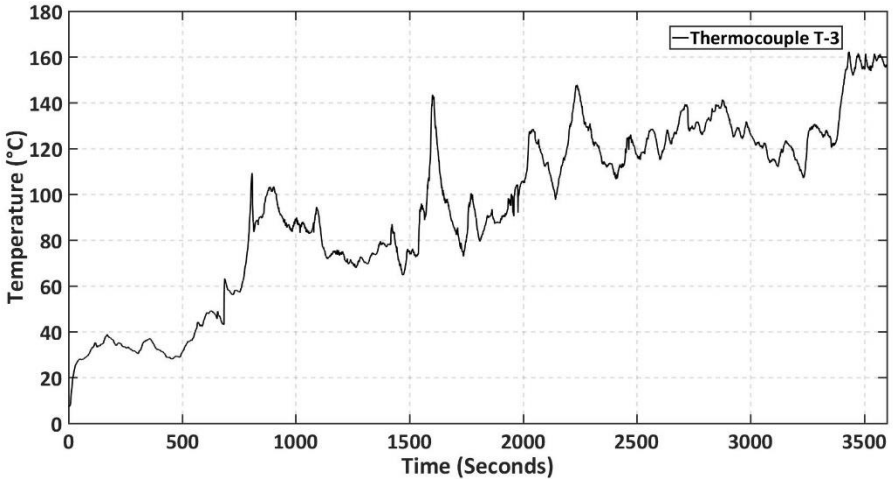

Figure 3-11 Thermocouple reading from T3

The maximum temperature recorded from T1, T2, and T3 are 400°C, 270°C, and 170°C, respectively. The uneven temperature distribution recorded between T1 and T2 was due to the wind drag occurred during the test. T3 reading was as expected less than T2 because it was not facing towards the fire. After the fire test, the girders were allowed to cool down and later tested for residual strength. The bearing pads were also tested to evaluate the change in their material properties which is discussed in detail in the next chapter.

Chapter 4

MATERIAL TESTING

After the fire test, the bearing pads were cooled down and were tested at COSMEC INC. The following standard tests were conducted on samples taken from the six bearing pads:

1. Hardness Test – ASTM D2240 (2015)
2. Shear Modulus – ASTM D4014 (2012)
3. Compression Set – ASTM D395 (2014)
4. Adhesion Strength – ASTM D429 (2014)

The values determined from the above-mentioned experiments are compared with control bearing pad whose properties are already known. All the tests are performed at ambient temperature of 23 ± 6°C. D4014 – 03(2012) – 'Standard Specifications for plain and steel-laminated elastomeric bearings for bridges' suggests the quality control limits for the material properties determined from these tests as shown in Table 4-1.The experiments are discussed in detail below.

Table 4-1 Acceptable test result limits

Acceptable test result limits	Test method Standard	Elastomer type - CR
Hardness Limits	D2240	45-75
Shear Modulus	D4014	±15%
Compression Set (After 22h at 100°C, max. %)	D395 - Method - B	35

4.1. Hardness Test

The experiment was conducted as per ASTM Standards – D2240 – 'Standard Test Method for Rubber Property – Durometer Hardness'.

This test method is based on the penetration of a specific type of indentation into a material under specific conditions. The indentation hardness is inversely proportional to the penetration. It is dependent on the elastic and viscoelastic behavior of the material. The geometry of the indentor and the applied force also influences the measurements. So, no simple relationship exists between the measurements obtained with one type of durometer and those obtained with another type of durometer. This test method is an empirical test intended primarily for control purposes. No simple relationship exists between indentation hardness by this test and any fundamental property of the material used.

The test specimens are generally 6.4mm (¼ in) thick. It is possible to pile several specimens to achieve the 6.4mm thickness, but one specimen is preferred. The type of durometer used is type A, so it is also called shore A hardness.

Experimental results are shown in Table 4-2.

Table 4-2 Temperature effect on hardness

Sample	Hardness (Shore A)	% difference compared to control bearing pad
Control	57	
1-1	56	-1.75
1-2	60	5.2
2-1	57	0
2-2	59	3.5
3-1	60	5.2
3-2	59	3.5

The fire load is expected to increase the crystallinity of elastomer and hence increase the hardness. Choi et al. (2005) has proposed empirical equations to predict the increase in hardness which accounts for time and amplitude of fire load, but it depends on sample size. Establishing those equations is beyond the scope of this research. From the test results the maximum increase in hardness is below 10%, also the sample was taken from the exterior layer where the temperature effect is maximum. Most of the interior part is almost unaffected. The maximum change of hardness value is also within the quality control limits as shown in Table 4-1. Hence this property change in this experiment is not significant to affect the overall performance of bearing pad.

There is no specific pattern in the change of hardness of elastomer from above results. This is due to uneven distribution of heat.

4.2. Shear Modulus

It is the most significant property of the bearing pad. As bearing pads are designed to accommodate horizontal and vertical deformations, accurate estimation of shear stiffness is crucial factor affecting the performance of bearing pad.

The standard used is ASTM D4014 – 'Standard Specifications for Plain and Steel Laminated Elastomeric Bearings for Bridges'. Shear Modulus is calculated from the shear force-extension curve after conditioning the sample to a cyclic loading up to 50% shear strain for five times in order to reach a stabilized stress-strain behavior. In the sixth cycle the stress corresponding to 25% strain is multiplied by four to find the shear modulus as shown in Figure 4-1.

A quadruple shear test specimen shall consist of four identical blocks of elastomer bonded to rigid plates as shown in Figure 4-2. They all are of equal thickness and the width and length no less than four times the thickness. The sample in six-

successive loading and release cycle subjected to a deformation equal to the average block thickness, T and then the shear modulus is calculated from equation 4-1.

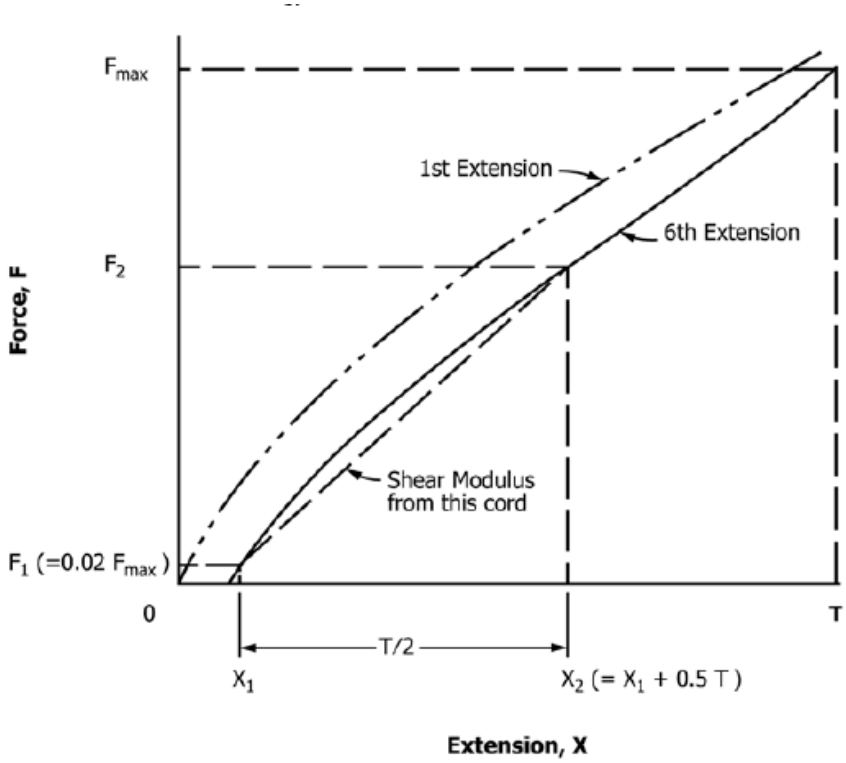

Figure 4-1 Shear Test Force-Extension Curves [D4014]

Shear modulus G is calculated as:

$$G = \frac{2(F_2 - F_1)}{A} \qquad 4\text{-}1$$

Where

T = Thickness of sample

F_{max} = Force corresponding to 50% strain in sixth cycle

F_1 = 2% of the maximum force on the sixth cycle

X_1 = Strain corresponding to force F_1 in sixth cycle

$X_2 = X_1 + 0.5T$

F_2 = Force corresponding to strain X_2

A = Area of cross section of one block of specimen

Therefore $X_2 - X_1$ corresponds to 25% strain.

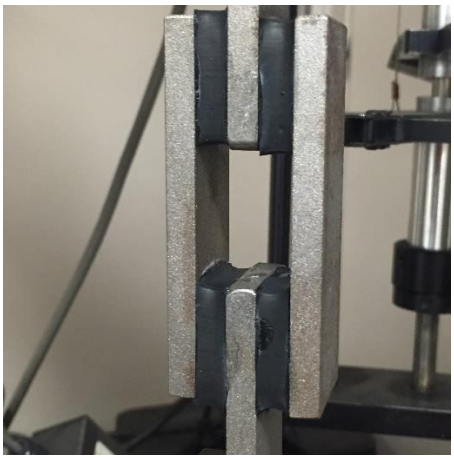

Figure 4-2 Shear Test Sample

Summary results is presented below

Table 4-3 Temperature effect on shear modulus

Sample	Shear Modulus MPa (psi)	% difference compared to control bearing pad
Control	0.78 (113.9)	
1-1	0.83 (120.6)	+5.88
1-2	0.86 (124.8)	+9.57
2-1	0.86 (124.4)	+9.22
2-2	0.83 (120.8)	+6.05
3-1	0.99 (144.0)	+26.43
3-2	0.87 (126.5)	+11.06

As elastomer hardens the shear modulus is expected to increase after cooling down. The maximum change in shear modulus is about 26% and minimum of 5.88% compared with control bearing pad sample. So, except for sample 3-1 all other samples are within the quality control limits mentioned in Table 4-1. The uneven changes are due to fact of uneven heating of bearing pads.

4.3. Compression Set

It is intended to determine the ability of the rubber material to retain its elastic property after prolonged loading. It is done in accordance with D395 – Standard Test Methods for Rubber Property – Compression Set.

There are two test methods –

A. Compression under constant force in air.

B. Compression under constant deflection in air.

Unless mentioned usually Method B – 'Constant Deflection' is adopted. The sample are cut in the shape of cylinders as shown in Figure 4-3. The dimensions of the samples are: thickness is 12.5mm, diameter is 29mm. These samples are placed between plates of compressive device with spacer bars on each side. The device is then locked to maintain a constant deflection. The amount of compression applied shall be approximately 25%. The whole device is then maintained for 22 hours at elevated temperature of 100°C. After that the samples were cooled and the final thickness was measured. Compression set is expressed as:

$$C_B = \frac{t_o - t_i}{t_o - t_n} * 100 \qquad 4\text{-}2$$

Where

C_B = compression set expressed as percentage of the original deflection

t_o = original thickness of specimen

t_i = final thickness of specimen

t_n = thickness of the spacer bar

Figure 4-3 Compression set samples

Table 4-4 Temperature effect on compression set

Sample	Compression Set %	% difference compared to control bearing pad
Control	9	
1-1	14	55.5
1-2	12	33.3
2-1	12	33.3
2-2	14	55.5
3-1	34	270
3-2	18	100

As seen from Table 4-4 compression set suffered maximum degradation due to fire. It means that rubber has lost its property to regain its original shape. This must do with the microstructure of the elastomer. As discussed in section 2.4.3, elevated temperature causes scission and formation of new crosslinks. This lead to the permanent set of the elastomer which is responsible for increased compression set. The maximum change measured is about 270% and minimum is about 33%. This shows a wide range of change of material property possible in elastomer. There can't be any simple explanation for this change as it depends on many factors like scission and crosslinking of polymer networks, temperature history, location etc.

From performance point of view this parameter is not much of direct significance as the bearing pads are not expected to return to its original state anytime during its service. Though test is meant to evaluate the long-term effects of applied stress or strain but NCHRP 449 (2001) recommends a direct full-scale creep test to evaluate the long-term performance of bearing pad. In NCHRP 449 (2001) it says 'The ASTM D395-89 set test is more suitable for applications such as seals where recovery of deformation may be important, rather than bridge bearings were creep is more important. So, for bridge bearings, the test is more of a quality control test because the results are sensitive to cure.' So, this test is recommended to be eliminated from AASHTO M251 by NCHRP - 449 (2001) report.

4.4. Adhesion Strength

This test covers the procedures for determining the static adhesion strength of rubber to rigid materials. It is performed as per ASTM D429 – 'Standard Test Methods for Rubber Property – Adhesion to Rigid Substrates'. Here test method – B – '90° Stripping Test – Rubber part assembled to one metal plate' is adopted. The result is obtained by

measuring force required to separate a rubber from the metal surface. The rubber strip is separated from the metal plate by 90 degrees as shown in

Figure 4-4.

The standard test specimen shall be a strip of rubber which has following dimensions

6.3 ± 0.1 mm (0.250 ± 0.005 in.) – thickness

25 ± 0.5 mm (1.000 ± 0.02 in.) – width

125 mm (5 in.) - length adhered to face of metal strip

The test specimen is prepared so that a bonded area of 25 by 25 mm (1 by 1 in.) is fixed approximately in the middle of the metal member as shown in Figure 4-5. The sample is cut from the bearing pad directly and tested for its adhesion strength.

The test specimen is symmetrically placed in the jaws attached and a power-driven test machine equipped to produce a uniform rate of grip separation at 50 mm (2.0 in.)/min. The force required for failure is recorded and the summary of results is presented in Table 4-5.

Figure 4-4 Adhesive Strength of elastomer

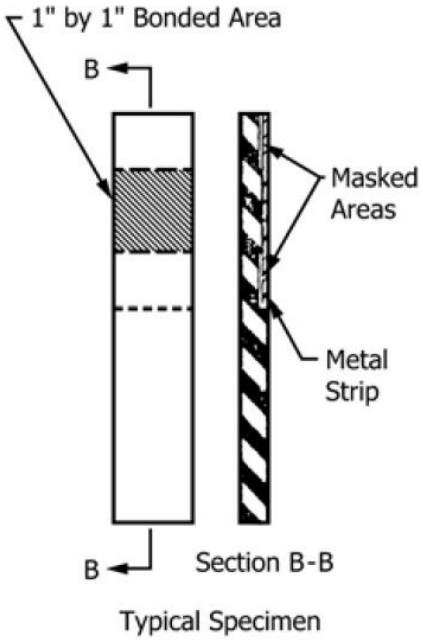

Figure 4-5 Typical Specimen for Adhesion Test

Table 4-5 Adhesion strength before and after the fire test

Sample	Adhesion Strength MPa (psi)	% difference compared to control bearing pad
Control	0.64 (93.91)	
1-1	0.78 (113.45)	20.8
1-2	0.66 (96.06)	2.3
2-1	0.72 (105.73)	12.6
2-2	0.76 (110.44)	17.6
3-1	0.47 (68.99)	-26.5
3-2	0.73 (105.79)	12.5

From results, it is seen that adhesion strength has increased after subjecting it to fire, except for sample 3-1. The increase in strength is because of hardening of elastomer

due to crystallization. But decrease in strength is may be because of degradation of elastomer beyond a certain point where there could be formation of micro cracks in the structure.

Chapter 5

NUMERICAL MODELLING

A numerical modeling scheme is developed to verify its accuracy in finding the shear strains produced under different loading patterns. Also, to perform a thermo-mechanical analysis to superimpose thermal shear strains on the mechanical strains produced in bearing pad. This is due to linear expansion of elastomer and steel when exposed to different temperatures over time. In mechanical analysis, the bearing pad is modelled in a 2D plane. Initially the bearing pad was modelled in 3D but the model was not stable at higher compressive loads due to near incompressibility property of elastomer. So, it was modeled in 2D and its results are close to the results from 3D model. The mechanical properties of elastomer are modelled as linear elastic and compared with hyperelastic model. Various loads as compression, shear and rotation are applied on the bearing pad and various parameters mentioned in section 2.1 are studied.

For the thermo-mechanical analysis, the thermocouple data from fire test was used to obtain nodal temperatures at different time steps. Then nodal temperatures are then used to find the thermal strains generated due to expansion of elastomer and steel. These thermal strains are then superimposed with the mechanical response due to applied external stresses. Later a parametric study was conducted by exposing the bearing pad to a uniform temperature for the time close to fire test i.e., one hour at 50°C, 100°C, 150°C and 200°C. The scope of this research was only to study the effect of temperature on the elastomer below 200°C, where there is no significant damage in the internal structure. Above 175°C-200°C range there occurs thermal degradation in elastomer (Alok,2000), and the model should consider scission and crosslinking of polymer chains (Alan, 2003) which is beyond the scope of this research.

The bearing pad dimensions and properties used in the fire test is shown in Table 5-1. It is subjected to various deformation modes as mentioned in

Table 5-2. Though the deformation modes are applied separately on bearing pad, but the linear superposition is justified due to the linear approximation of elastomer behavior.

Table 5-1 Bearing Pad Dimensions

Length	0.5334 m (21 inches)
Breadth	0.2286 m (9 inches)
Total height	0.076835 m (3.025 inches)
Total no. of steel laminates	5
Thickness of steel laminate	0.002667 m (0.105 inches)
Outer layer thickness of elastomer	0.00635 m (0.25 inches)
Inner layer thickness of elastomer	0.0127 m (0.5 inches)
Number of internal layers of elastomer	4
Total height of elastomer (total)	0.0635 m (2.5 inches)
Total height of elastomer (excluding exterior layers)	0.0508 m (2 inches)
Shape factor for internal layer	6.3
Shape factor for external layer	12.6

Table 5-2 Deformation modes and surface conditions

Deformation modes
Compression (C)
Shear (S)
Rotation (R)

Detailed flow of the numerical analysis is presented below –

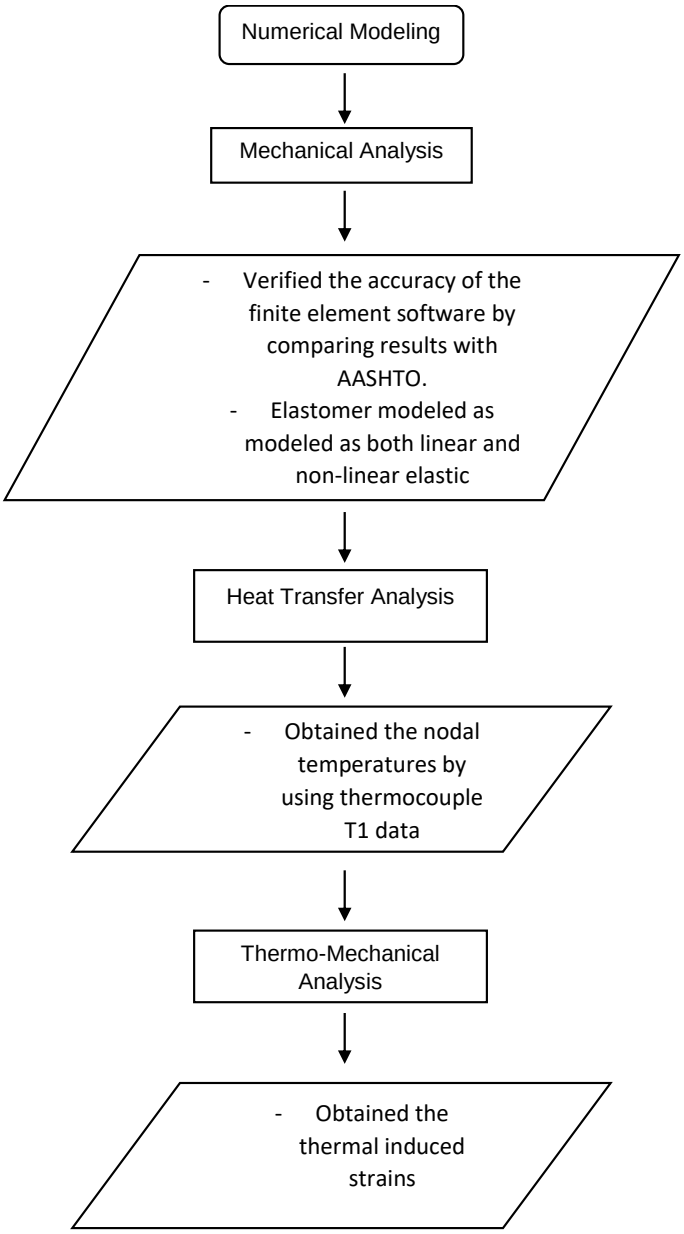

5.1. Mechanical Analysis

In mechanical analysis, the objective was to verify the capability of numerical model in accurately predicting the performance parameters mentioned in Table 2-1. The bearing pad is modelled as per the dimensions mentioned in Table 5-1. The steel shims are of ASTM A36 grade which are modelled as 'linearly elastic and perfectly plastic' as shown in Figure 5-1 and with the following properties:

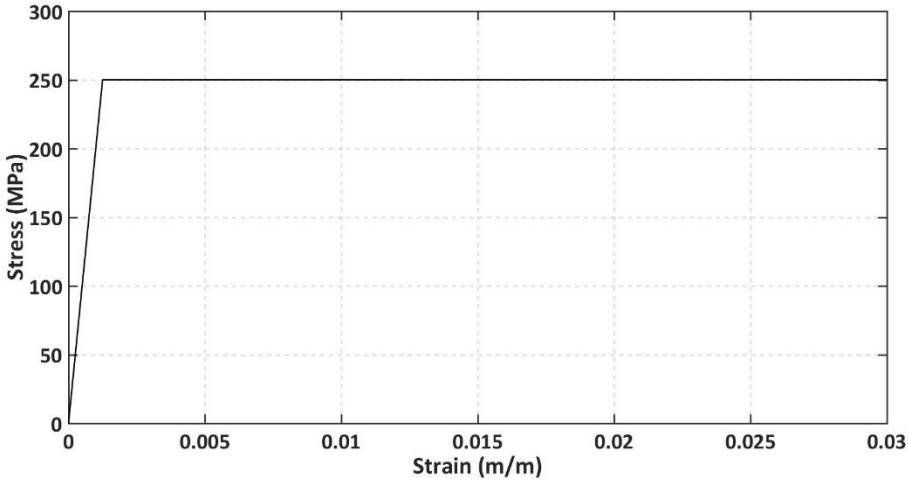

Figure 5-1 Stress-Strain for steel shims

- Yield stress = 250 MPa
- Modulus of Elasticity = 200GPa
- Poisson's ratio = 0.29 and
- Density = 7.85 Mg/m^3.

In nonlinear analysis, the elastomer was modelled as nonlinear, elastic, nearly incompressible material using 'Yeoh Model' with the material coefficients from NCHRP 12-68 (2006). The parameters are:

- Shear Modulus G = 0.689 MPa (100 psi)
- Bulk Modulus K = 2758 MPa (400 ksi)

- C_{10} = 344,470 Pa (49.961 psi)
- C_{20} = -6,216 Pa (0.901555 psi), and
- C_{30} = 292.09 Pa (0.042364 psi)

Where C_{10}, C_{20}, C_{30} are material constants as discussed in Section 2.4.1. The elastomer is also modelled as linearly elastic to compare the results with the hyperelastic model. Its properties in linearly elastic model as given by the manufacturer are shown below. Table 5-3 shows the material properties for different grades of elastomer.

- Poisson's ratio = 0.4999
- Density = 8.3 Mg/m^3.
- Young's Modulus – As mentioned in Table 5-3

Table 5-3 Elastic properties of different elastomer grades

Hardness (Shore A)	Young's Modulus E_o	Shear Modulus G
50	2.2 MPa (312 psi)	0.68 MPa (100 psi)
60	4.4 MPa (635 psi)	1.04 MPa (150 psi)
70	7.2 MPa (1040 psi)	1.69 MPa (245 psi)

In both nonlinear and linear analysis, elastomer is modeled using CPE8RH elements (8 node biquadratic plane strain quadrilateral, hybrid, linear pressure, reduced integration). These elements use hybrid formulation because when the poison's ratio is close to 0.5 conventional elements will lead to numerical instability. Steel shims are also modeled using same elements. Mesh dimension is sized to keep the aspect ratio below 5 as shown in Figure 5-2 and Figure 5-3

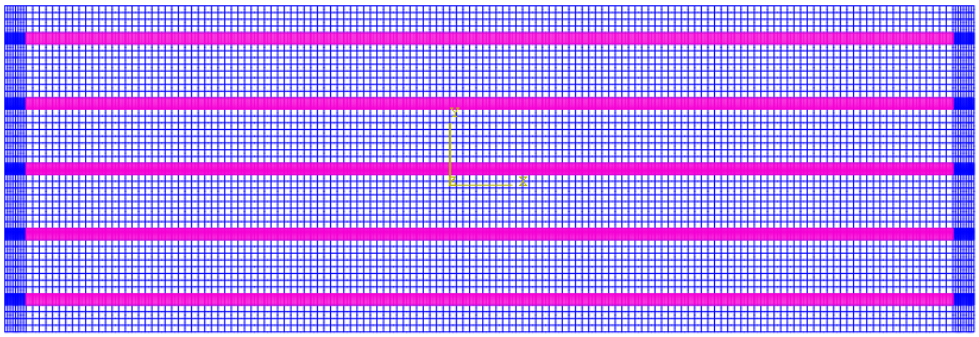

Figure 5-2 Mesh of bearing pad

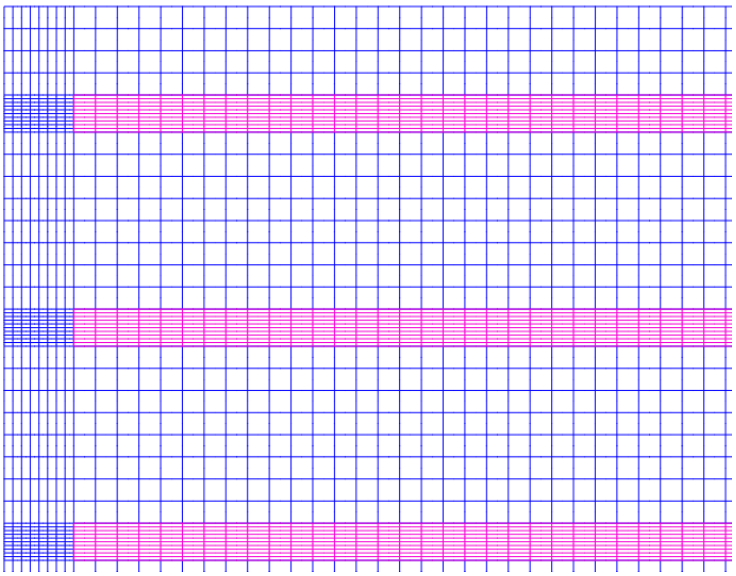

Figure 5-3 Close view of mesh of bearing pad

In mechanical analysis, the bearing pad is subjected to compression, shear and rotational deformations for 50 DURO elastomer grade and various performance parameters are studied which are explained in detailed below.

5.1.1 Compressive Load

A compressive load is applied on the top surface of bearing pad, which simulates the compressive stresses from the bridge girder. All the top nodes on which the

compressive load is applied are couple together so that the all nodes will have uniform vertical displacement. Typically, these stresses are in the range of 1.37MPa to 6.98MPa (200 – 1000 psi), which is the usual range in which the bearings are designed for. In the fire test performed in current project the bearing pads are subjected to a load of 1.53MPa – 2.2MPa. (222 psi - 320 psi).

A compressive load in the steps of 1.37MPa (200psi) are applied on the bearing pad up to 6.98MPa (1000 psi) and corresponding parameters obtained in each load case under different elastomer models are presented below.

5.1.1.1. Shear Strain

Shear Strain is the most important parameter bearing pads are designed for, hence it's precise estimation is very much needed for an efficient design. The applied compressive load on the bearing pad produces shear strains in the elastomer which linearly increases from the interior to the edges. Maximum shear strain in elastomer occurs the edge of the steel shim. Maximum shear stress was along the short direction of the bearing pad as there is less material to resist the stress in short direction and hence deforms more.

Table 5-4 presents the results from numerical simulation and from the AASHTO (2014) equations to find shear stress (using equation 2-1). Figure 5-4 shows the results from the software at load of 1.37Mpa under linear elastic model. Figure 5-5 shows the graphical representation of the results at various loads.

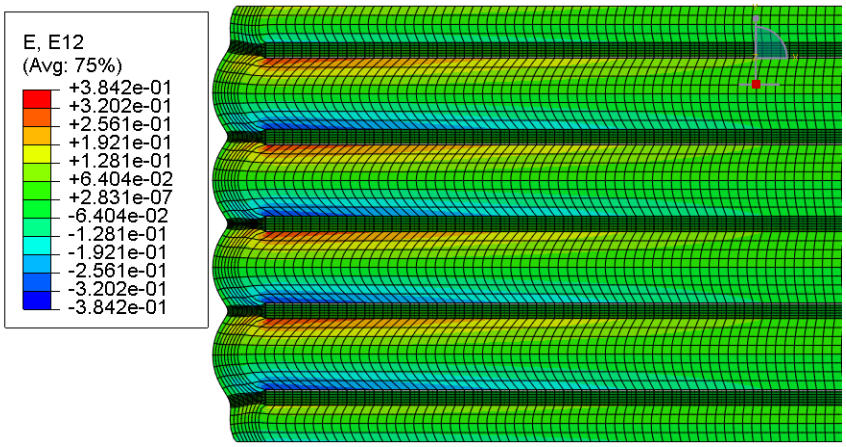

Figure 5-4 Shear Stress in elastomer under compression

Table 5-4 Shear strain in compression

Compressive Stress (MPa)	Max. Shear Strain in compression(m/m)		
	Linear Elastic (% change from AASHTO)	Hyperelastic (% change from AASHTO)	AASHTO formulae
1.37 (200 psi)	0.38 (-15.12%)	0.42 (-4.5%)	0.44
2.75 (400 psi)	0.77 (-15.43%)	0.66 (-26%)	0.89
4.13 (600 psi)	1.15 (-14.05%)	0.95 (-28.6%)	1.33
5.51 (800 psi)	1.54 (-15.03%)	1.18 (33.7%)	1.78
6.9 (1000 psi)	1.93 (-14.28%)	1.31 (41%)	2.22

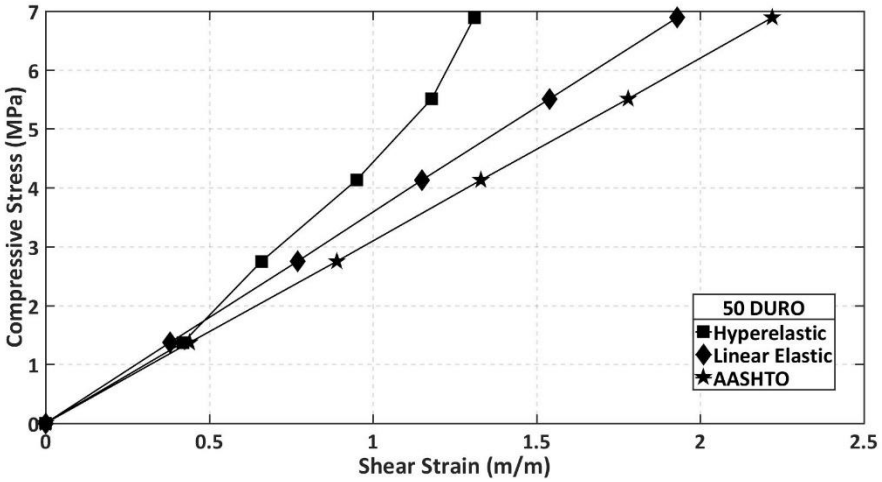

Figure 5-5 Shear Strain under compression

As it can be seen, the results from linear elastic model is close to the AASHTO (2014) predicted shear strain but less by about 13% and hyper elastic model results vary from 4 – 41% less than AASHTO (2014) depending on the applied stress. This is because AASHTO (2014) formulas are developed using the linearly elastic theory assumptions and did not consider edge cover (NCHRP 12-68 2006). So, as the edge cover also provides additional resistance to deformation its values are off by small amount but it is not very significant in linear elastic model. Whereas in hyperelastic model, the deviation is as high as 41% less than predicted shear stress, this is due to the non-linear response curve of the elastomer. This is highly dependent on the assumed material model and constants.

5.1.1.2. Axial Strain

TxDOT Example for Bearing Pad Design (2010) mentions that “Compressive deflection is usually not a concern from functionality standpoint since 4% to 5% range of deflection that most TxDOT standard pads undergo, yields a hardly noticeable 3/32″

vertical compression". This is because even vertical deflection up to 0.4 cm (5/32") is well within the limit to induce a "bump" at the end of the section in a bridge.

Axial strain under different compressive loads are presented in (at 200psi applied uniform compressive load)

Table 5-5 and corresponding output from software is shown in Figure 5-6. Figure 5-7 graphically presents the results summary.

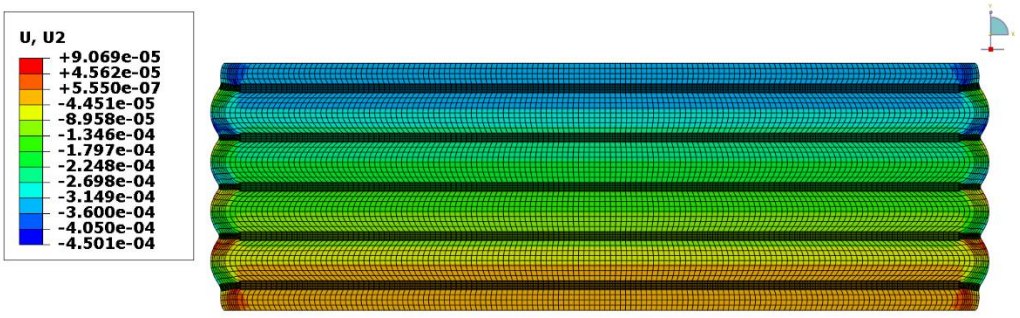

Figure 5-6 Vertical displacement under compressive stress (at 200psi applied uniform compressive load)

Table 5-5 Axial strain in bearing pad

Compressive Stress (MPa)	Axial Strain %		AASHTO equation	AASHTO curve
	Linear Elastic (% change from AASHTO eq.)	Hyper Elastic (% change from AASHTO eq.)		
1.37 (200 psi)	0.71 (0%)	0.68 (-4.2-%)	0.71	1.21
2.75 (400 psi)	1.42 (-0.6%)	1.33 (-7%)	1.43	2.28
4.13 (600 psi)	2.13 (-0.4%)	1.93 (-10%)	2.14	3.23
5.51 (800 psi)	2.85 (0%)	2.56 (-10%)	2.85	4.14
6.9 (1000 psi)	3.56 (0%)	3.19 (-11%)	3.56	4.99

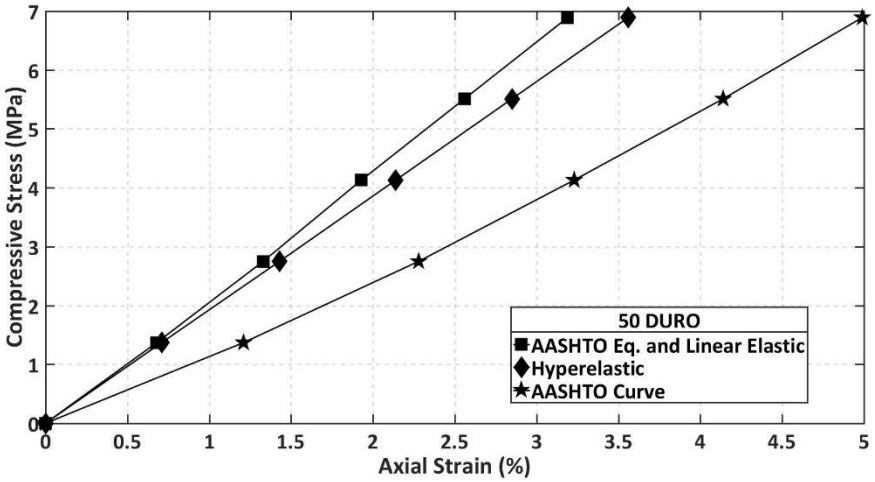

Figure 5-7 Compressive Strain under compressive deformation

As it can be seen from the results that AASHTO (2014) equation 2-18 yields close results compared with results from linear elastic model. Hyperelastic model yields a stiffer behavior and AASHTO (2014) curve Figure 2-4 results are too conservative.

Vertical deflection is very much dependent on the surface boundary conditions. AASHTO (2014) in its estimation of compressive strains assumed that top and bottom surface area remain constant (NCHRP 12-68 2006) i.e., all nodes are tied together. The compression stress strain curves for different shape factors in AASHTO (2014) also performed on samples which are restrained on top and bottom surface by placing them over a 400-grit sand paper as to ensure no slip during the test (McPherson 1956).

5.1.1.3. Bond Stress

The bond between steel and elastomer is modeled by defining cohesive stiffness coefficients. In bearing pad, steel and elastomer are vulcanized together to form a strong bond. Also in adhesion test, as per TxDOT 601- J the failure must occur in elastomer and not in elastomer/steel laminate. Hence, the stiffness coefficients values are adjusted upto

a point where the increase in frictional shear stress for a given load is negligible or almost constant. The bond stress between steel and elastomer is reported in Table 5-6. All these values are below 1.31 MPa. There is no significant change in bond stress from linear elastic and hyperelastic model and they are well below the limits.

Table 5-6 Bond stress under compressive load

Compressive Stress (MPa)	Bond Stress (MPa) (Max. 1.31MPa)		
	Material model		% change in Hyperelastic model compared with Linear Elastic
	Linear Elastic	Hyper Elastic	
1.37 (200 psi)	0.15	0.2	33
2.75 (400 psi)	0.35	0.4	14.3
4.13 (600 psi)	0.55	0.6	9
5.51 (800 psi)	0.75	0.8	6
6.9 (1000 psi)	0.9	0.99	10

5.1.1.4. Principal Strain

Maximum principal strains i.e., maximum uniaxial tensile strains are limited to 2 (200 percent) (Alok, 2000). This is because the strain range considered in the model are very small where elastomer stress-strain was approximated to be a linear.

Maximum principal strains occurred at the interface as shown in Figure 5-8. Its values at various compressive loads are presented in Table 5-7. As it can be observed, most of its values are well below the limits.

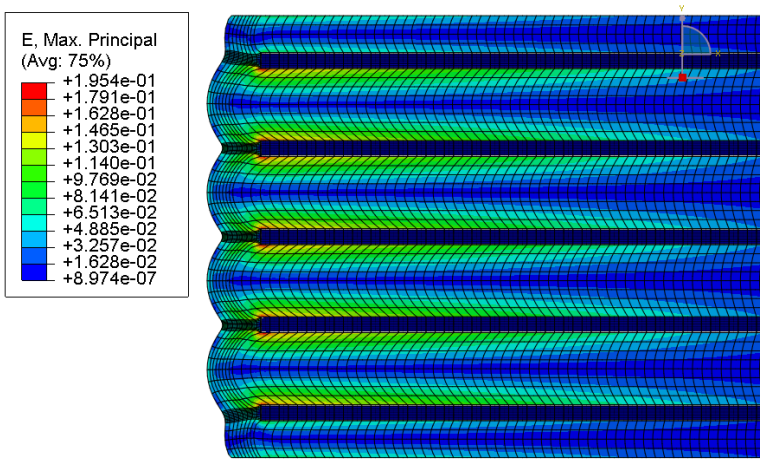

Figure 5-8 Max. Principal Strain

Table 5-7 Maximum Principal Strain

Compressive Stress (MPa)	Principal Strain (m/m) (Max. 2)	
	Material model	
	Linear Elastic	Hyper Elastic
1.37 (200 psi)	0.13	0.13
2.75 (400 psi)	0.27	0.28
4.13 (600 psi)	0.40	0.45
5.51 (800 psi)	0.54	0.67
6.9 (1000 psi)	0.68	0.89

5.1.1.5. Von Mises in Steel

Figure 5-9 show the plot of von Mises stress in steel laminates. Maximum von Mises stresses occurs in the centroid of the model and all their values are reported in Table 5-8. All the values obtained are well within the limits. The difference of values between different material models are not more than 2%. Hence failure by yielding of steel plates is not a critical issue.

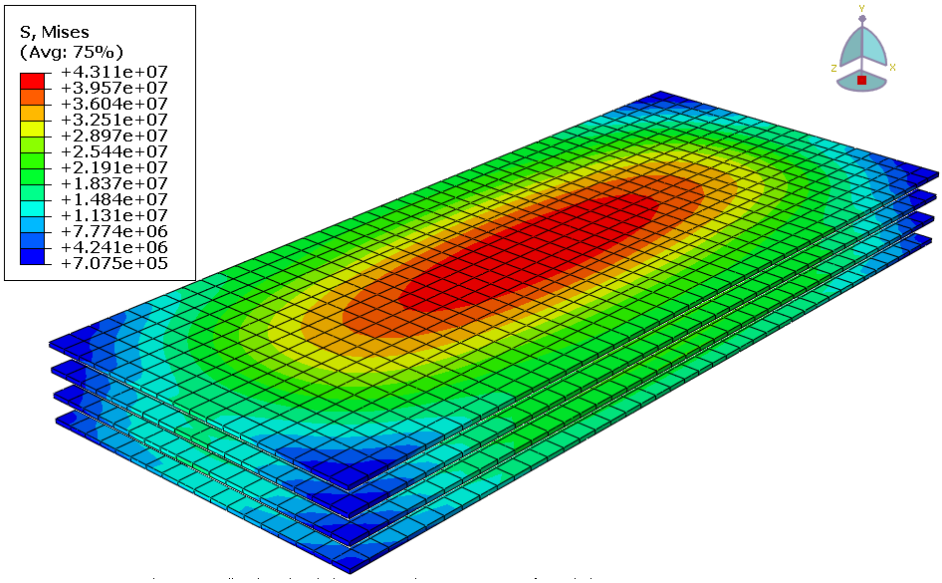

Figure 5-9 von Mises in Steel

Table 5-8 von Mises in Steel

Compressive Stress (MPa)	Von Mises MPa (<235MPa)	
	Linear Elastic	Hyper Elastic
1.37 (200 psi)	14.3	14.3
2.75 (400 psi)	28.7	28
4.13 (600 psi)	43	42
5.51 (800 psi)	57	56
6.9 (1000 psi)	71.1	73

5.1.1.6. Hydrostatic Tensile Stress.

The applied compressive load produces hydrostatic stresses in the elastomer. Most of the stresses are compressive in the middle but are tensile towards the edges as shown in Figure 5-10, which shows the quarter model of complete bearing pad. The maximum hydrostatic tensile stresses occur at the edge of steel shim as shown in Figure

5-11. These stresses are limited to 3G for design purpose, because it causes internal cavitation in elastomer as it reaches to 3G (Gent & Lindley 1959). A compressive stress of 1.02GS would be sufficient to produce the stress of 3G, hence the applied compressive stress is limited to 1.02GS in AASHTO (2014) Method-A design. The summary of maximum hydrostatic stress under different loads is presented in Table 5-9.

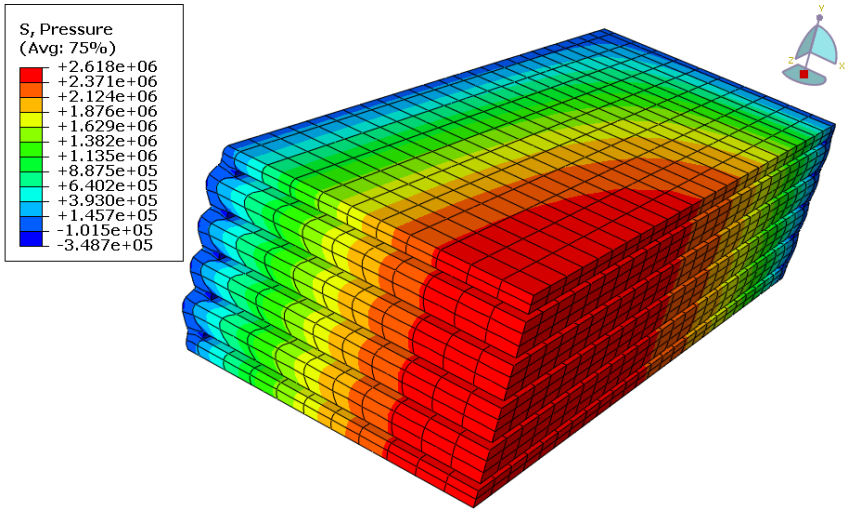

Figure 5-10 Hydrostatic Stress in Elastomer

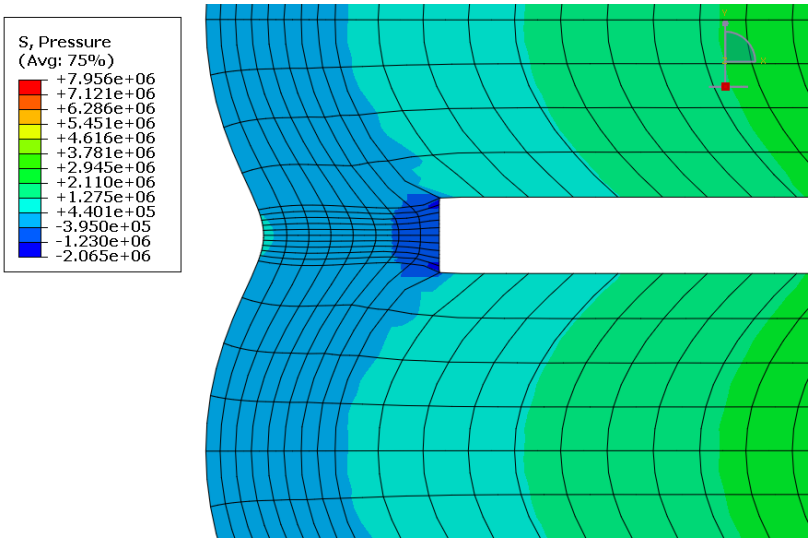

Figure 5-11 Hydrostatic Tensile Stress in Elastomer

Table 5-9 Hydrostatic Tensile Stress in Elastomer

Compressive Stress (MPa)	Hydrostatic Tensile Stress (MPa)	
	Linear Elastic	Hyperelastic
1.37 (200 psi)	0.54	0.47
2.75 (400 psi)	1.08	0.92
4.13 (600 psi)	1.63	1.39
5.51 (800 psi)	2.17	1.88
6.9 (1000 psi)	2.72	2.32

In this model, the averaged shape factor is 7.56, hence the limiting hydrostatic stress of 2MPa (3G = 2MPa) is expected when applied compressive stress reaches 1.02GS, which is 5.24MPa. This value is close to the ABAQUS results in linear elastic model. In linear model, the 2MPa hydrostatic tensile stress is reached at 5.07 MPa applied compressive stress, which is approximately 0.98GS. From hyperelastic model the corresponding stress is reached at 5.89MPa, which approximately 1.14GS.

In design method-A the applied compressive should be less than 1.02GS, but in method-B the design is controlled by limiting the shear strains produced under different deformations possible in bearing pad to be less than 5. Also, the shear strain produced only by compressive stress in further limited to 3.

AASHTO (2014) formulae for shear strain under compressive load is

$$\gamma_a = D_a \frac{\sigma_s}{G\, S_i} \qquad 5\text{-}1$$

Where D_a = 1.4, when $\sigma_s = 1.02GS$ the value of shear strain is equal to 1.428. This value is far less than the limit suggested by AASHTO (2014), which is 3. This is because the

limit 1.02GS proposed in method-A is far too conservative. From the experiments conducted in NCHRP12-16(2006) the de-bonding occurred in the stress range of 4.7GS to 7.8GS. So, in design method B this limit is apparently pushed to a higher value, i.e., by limiting the shear strain in compression to 3 the allowable compressive stress is 2GS and corresponding hydrostatic tensile stress is 6G.

5.1.2 Shear Deformation

A shear deformation is applied at the top surface of the bearing pad and corresponding shear stiffness values are reported from the numerical simulation under linear elastic and hyperplastic models. AASHTO (2014) recommends using the shear modulus of bearing to be equal to the shear modulus of elastomer. This is because steel shims are horizontal, so they may not have significant contribution to the shear modulus of whole bearing pad. The shear modulus of elastomer is taken as twice the stress required to produce a shear strain of 0.5.

In numerical simulations, a displacement boundary condition corresponding to 50% of the total thickness of elastomer is applied on the top surface nodes of elastomer while bottom nodes are fixed. Shear strains corresponding to those displacements are used to find the shear modulus as shown in Figure 5-12. From numerical simulations, the shear stiffness values of bearing pad were found to be same as that of elastomer in both elastic and hyperelastic model assumptions as shown in Table 5-10. This is because the coefficients in hyperelastic model are scaled based on shear strains.

Table 5-10 Shear Stiffness of Bearing Pad

	Material Model		AASHTO
	Elastic (% difference from AASHTO)	Hyperelastic (% difference from AASHTO)	
Shear Stiffness (MPa) @50% Shear Strain	0.64 (6%)	0.64 (6%)	0.68

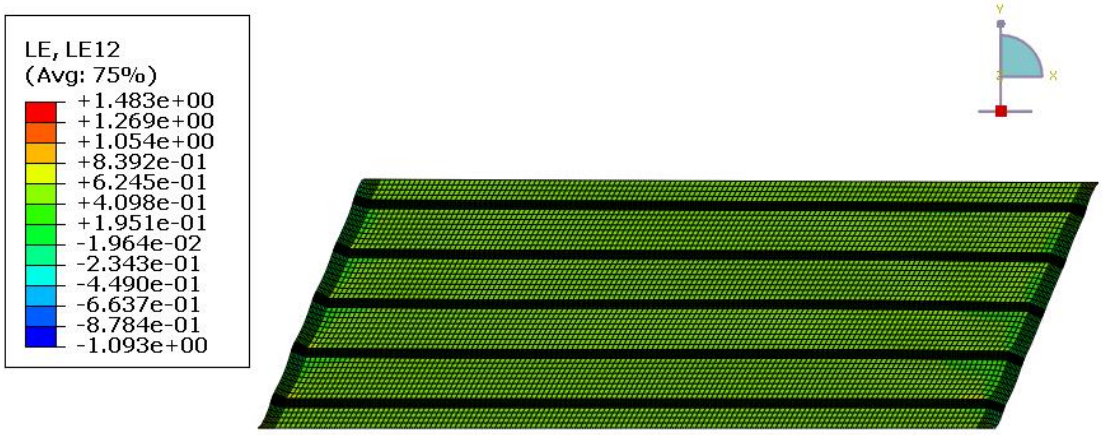

Figure 5-12 Shear Strain in Bearing Pad

5.1.3 Rotational Deformation

In AASHTO latest edition 2014 there is no limit for maximum rotation that can be applied, however if there are too large rotations, other bearings as pot bearings are preferred. However, in AASHTO (2014) 14.4.2.1 – total maximum rotation is defined as sum of rotation caused by service loads and 0.005 rad. (for uncertainties). Suggested rotation per layer is 0 to 0.01 radian (NCHRP12-16(2006). Hence a rotation of 0.005, 0.01, 0.015 and 0.02 is applied on the bearing pad. Rotation is applied on the top surface nodes which are coupled together. Figure 5-13 shows the rotational deformation of bearing pad and shear stresses developed in elastomer. The maximum shear strain occurs at the edges, interface between steel and elastomer.

Table 5-11 summarizes the results obtained from rotational deformation for the elastomer elements. As seen from the results shear strains obtained from numerical simulation under linear and nonlinear elastic model is close to the AASHTO (2014) predictions. All other parameters like von Mises and others from the hyperelastic model are well within the limit mentioned in section 2.

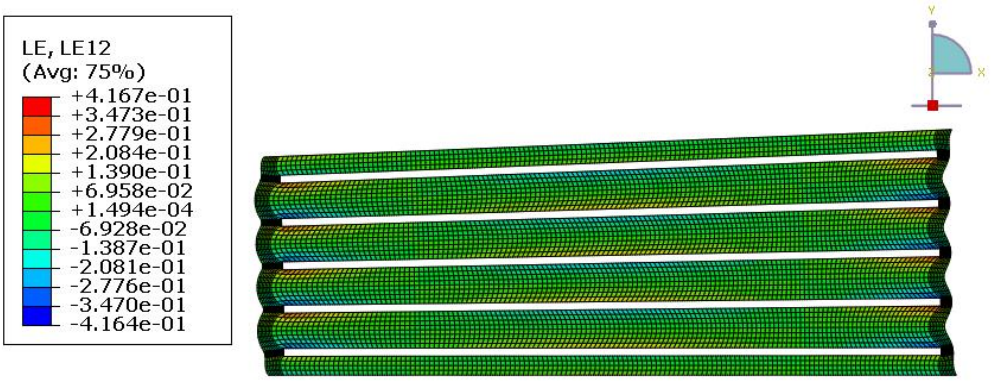

Figure 5-13 Rotational deformation of bearing pad

Table 5-11 Results from rotational deformation

Roatation Angle	Shear Starin		von Mises (Mpa)	Hydrostatic Stress (Mpa)	Principal Strain (m/m)	AASHTO - Shear Strain (m/m)
	Linear Elastic (%Diff. from AASHTO)	Hyperelastic (%Diff. from AASHTO)				
0.005	0.58 (-3%)	0.6 (0%)	15.2	3	0.2	0.6
0.01	1.17 (-6.4%)	1.2 (-4%)	30	5.9	0.4	1.25
0.015	1.76 (0.5%)	1.8 (2.8%)	45	8.9	0.6	1.75
0.02	2.35 (-6%)	2.4 (-4%)	60	12	0.8	2.5

It can be observed from results that predicted shear strain from AASHTO (2014) and from numerical simulation are in good agreement in both the material models.

5.2 Heat Transfer and Thermo-Mechanical Analysis.

Elastomer is a poor conductor of heat compared to metals. Hence, it cannot easily dissipate the heat developed. Also, thermal expansion coefficient of elastomer is very high, usually as a thumb rule it is assumed to be ten times higher than steel (Bhowmick 2008). So, a high thermal coefficient coupled with the high bulk modulus creates a situation where a very high thermal pressure could be developed if elastomer is confined and subsequently heated (Dorfmann 1991). Hence there can be significant thermal strains induced in elastomer when exposed to high temperature. To find these thermal strains a thermos-mechanical analysis model was developed.

To perform the thermo-mechanical analysis first nodal temperatures must be determined. Hence the bearing pad is modeled where its vertical exposed surfaces are subjected to radiative and convective heat transfer using the thermocouple data of T-1 from the fire test. The following material properties were used for modeling the elastomer (Mandal et. al. 2014):

- Thermal conductivity = 0.19 W/m K
- Coefficient of thermal expansion = 22×10^{-5} m/m°C
- Specific heat = 1802 J/Kg K at 23°C and 2635 J/Kg K at 200°C

The conductivity of elastomer is very low compared with steel and its variation with temperature is negligible in the domain of 25-200°C (ASDTR61-234).

Thermal properties of steel considered in the modeling according to Eurocode (2005) are:

- Coefficient of thermal expansion = 12×10^{-5} m/m °C
- Thermal conductivity and specific heat as shown in Table 5-12 and Table 5-13.

Table 5-12 Thermal Conductivity of Steel Vs temperature

Thermal Conductivity (W/m K)	Temperature (°C)
53.3	25
50.7	100
47.3	200

Table 5-13 Specific Heat of Steel Vs Temperature

Specific Heat (J/Kg K)	Temperature (°C)
440	25
448	100
530	200

A convective heat transfer coefficient of 50 W m^{-2} K^{-1} and 9 W m^{-2} K^{-1} was used for fire exposed and unexposed surfaces, respectively. (EN 1992-1-2 2002).

The governing equation for transient heat conduction is given by (SFPE 2016):

$$\rho c \frac{\partial T}{\partial t} = \frac{\partial}{\partial x}\left(k \frac{\partial T}{\partial x}\right) + \frac{\partial}{\partial y}\left(k \frac{\partial T}{\partial y}\right) + \frac{\partial}{\partial z}\left(k \frac{\partial T}{\partial z}\right) + \dot{Q}_v''' \qquad 5\text{-}2$$

where k, ρ and c denote the temperature-dependent thermal conductivity, density and specific heat capacity, respectively; $\dot{Q}_v'''$ is the inherently generated heat; and t is the time variable.

To solve the governing differential equation initial condition and boundary condition needs to be specified. The initial condition is given by:

$$T(x,y,z)|_t = T_o(x,y,z) \qquad 5\text{-}3$$

Where: (x,y,z) is the ambient temperature of the test specimen.

The sides of the bearing pad were directly exposed to the pool fire. Thus, heat is exchanged between the fire and these surfaces through convection and radiation, which can be expressed using Robin boundary condition (Purkiss 2007):

$$\dot{h}_{net} = \alpha_c(\theta_g - \theta_m) + \varepsilon_m \varepsilon_f \sigma \left[(\theta_g + 273)^4 - (\theta_m + 273)^4\right] \qquad 5\text{-}4$$

Where: $\dot{h}_{net}$ is the net heat flux; α_c is the convective heat transfer coefficient. Its value is 50 W/(m^2. K) for hydrocarbon fire and 9 W/(m^2. K) for unexposed surface (EN 1992-1-2 2002); θ_g is the fire temperature; θ_m is the surface temperature of the structural member; σ is the Stefan–Boltzmann constant and is equal to 5.67x10-8 W/(m^2. K^4); ε_m and ε_f are the emissivity of the exposed surfaces and the fire, respectively. As per the provision of EN 1992-1-2 (2002), ε_m=0.9 and ε_f=1.0. (Isidoro Matinez 2017)

The elastomer and steel both are modeled using DC3D8 (eight-node solid) elements. Tie constraint was used to model the bond between elastomer and steel. The temperature reading from thermocouple T-1 is used to model the transient temperature amplitude. The hyperelastic material model mentioned in section 5.1 is used for heat transfer analysis and thermomechanical analysis.

Figure 5-14 show the nodal temperature data obtained after heat transfer analysis of full scale model. Maximum recorded temperature at the end of analysis after 3600 seconds is 289.6°C which is at the corners and most of the interior part is around 51°C.

Figure 5-15 shows the plot of nodal temperatures at different sections. Nodal temperatures reported are for the interior layer of elastomer. Different sections on which nodal temperature reported are:

a. On the face of the elastomer (along the width)
b. At a distance 1-inch interior from the exterior face and
c. At the middle of bearing pad.

From

Figure 5-15, on the face of bearing pad, most of the nodal temperatures are about 240°C. At one-inch distance, it is about 70°C and in the interior part it is almost 51°C.

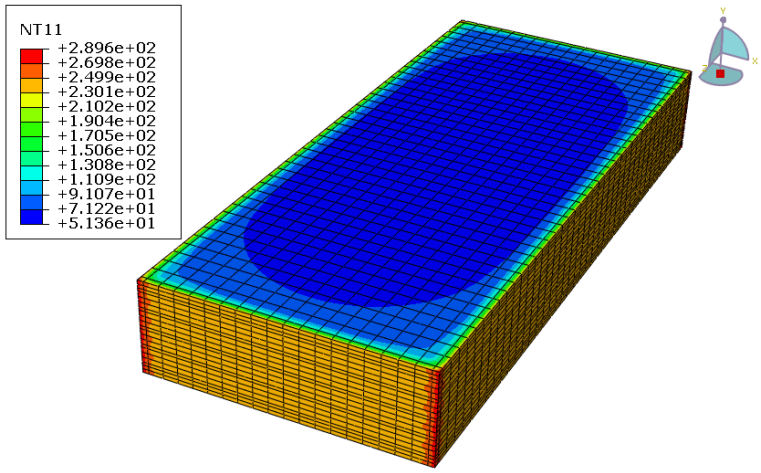

Figure 5-14 Nodal Temperature Distribution

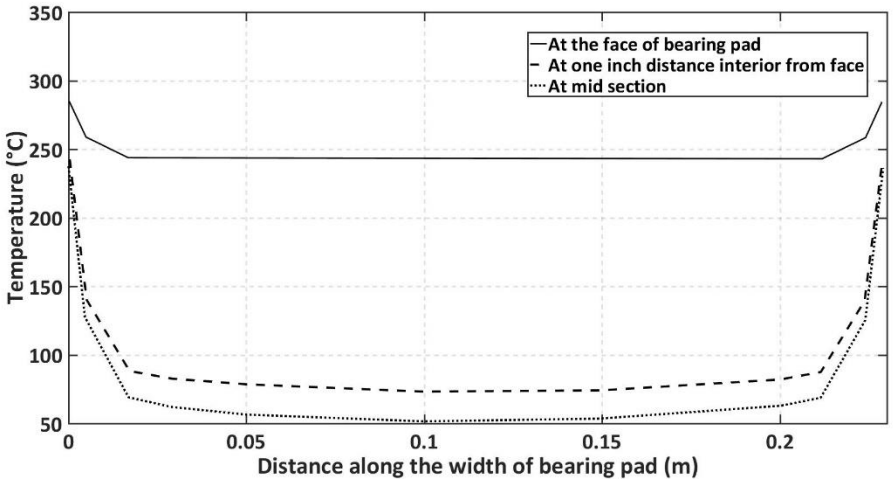

Figure 5-15 Nodal Temperature Distribution at different Sections

The bearing pad when exposed to temperatures the heat is transferred in all three dimensions. But however as mentioned previously in mechanical analysis, 3D model poses severe numerical instability. To overcome this challenge heat transfer analysis was also performed on a 2D model and the nodal temperatures obtained are compared with 3D model. It is modeled with boundary conditions like that of full scale model except that the heat transfer is modeled only on two exterior faces on right and left side. Figure 5-16 shows the temperature distribution on 2D model and Figure 5-17 shows the comparison of the nodal temperatures taken at mid-section from 3D and 2D model. It is found that they are very close. This is because the thermal conductivity of elastomer is very low and has very high specific heat. Hence it could be justified to perform the thermo-mechanical analysis by using the nodal temperatures from heat transfer performed on 2D model even though heat propagates in 3D.

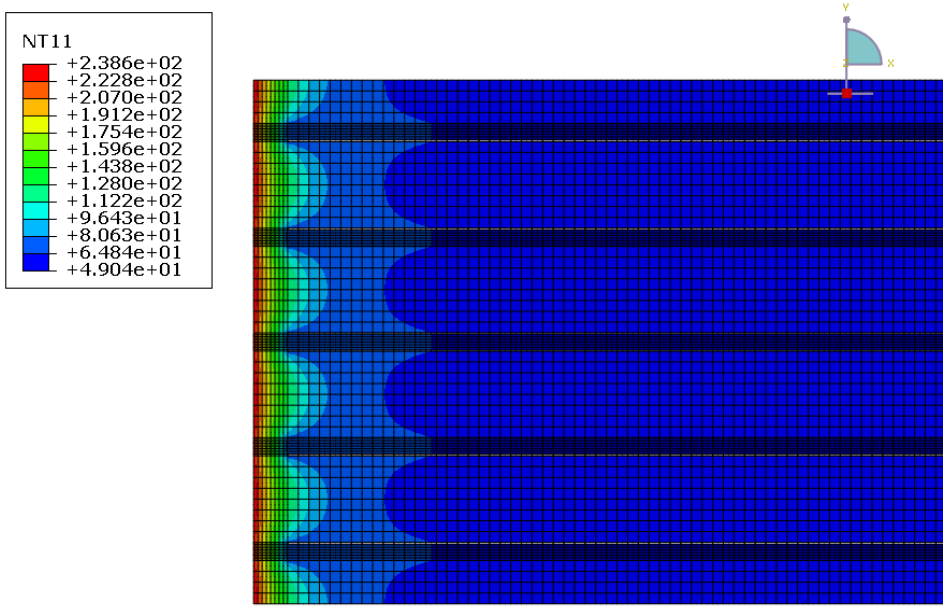

Figure 5-16 Nodal Temperatures from 2D model (at t = 3600 sec.)

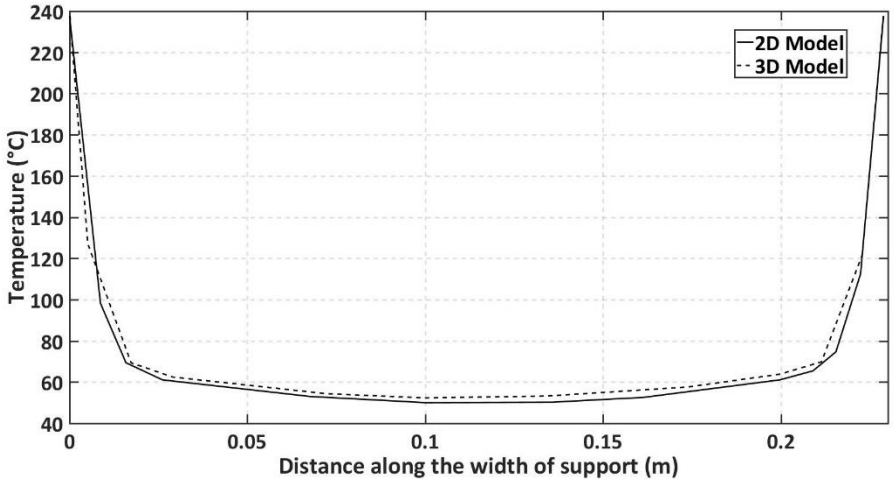

Figure 5-17 Comparison of 2D and 3D Model Nodal Temperatures (at t=3600 seconds)

The results of thermo-mechanical analysis by exposing the bearing pad to thermocouple data is shown in Table 5-14

Table 5-14 Bearing pad parameters after subjecting to hydrocarbon pool fire

Compressive Stress (MPa)	Shear Strain (m/m)		Hydrostatic Tensile Stress (MPa)		Bond Stress (MPa)	
	At ambient Temperature	After Fire Exposure (% change from ambient)	Before Heat Transfer	After Fire Exposure (% change from ambient)	Before Heat Transfer	After Fire Exposure (% change from ambient)
1.37 (200 psi)	0.42	0.73 (74%)	0.47	1.01 (115%)	0.2	0.52 (106%)
2.75 (400 psi)	0.66	1.03 (56%)	0.92	1.56 (70%)	0.4	0.79 (97%)
4.13 (600 psi)	0.95	1.24 (31%)	1.39	2.04 (47%)	0.6	0.96 (60%)
5.51 (800 psi)	1.18	1.37 (16%)	1.88	2.50 (33%)	0.8	1.20 (50%)
6.9 (1000 psi)	1.31	1.43 (9%)	2.32	3.02 (30%)	0.99	1.39 (40%)

Shear strain increased by 74% at lower compressive stress values and by 9% at higher compressive stress values. This is because at higher loads mechanical strains dominate the thermal strains. Hydrostatic tensile stress and bond stress by 115% and 106% respectively at lower compressive stress. At higher compressive stress, the increase is by 30% and 40% for hydrostatic stress and bond stress respectively as shown in Table 5-14.

5.3. Parametric Study

Elastomers are available in different grades based on their hardness. Commonly available grades are 50, 60, 70 Duro which has different material properties as shown in Table 5-3. These different grades are achieved by adding fillers and other materials during the manufacturing process. Most commonly used elastomer grade in bearing pads is 50 Duro.

A parametric study was conducted on different grades of elastomer considering the effect of fillers and exposing them to different ranges of temperatures.

Fillers affect the thermal properties of elastomer. The thermal properties used are shown in Table 5-15 and

Table 5-16. Though the exact properties depend on the proportions of each filler materials, conservative values are used to study its maximum effect.

Table 5-15 Variation of thermal conductivity of elastomer due to fillers (ASDTR61-234, Oggermuller (2008)

Condition	Thermal Conductivity
Without filler	0.19 W/mK
With filler	0.45 W/mK

Table 5-16 Variation of specific heat of elastomer due to fillers (Mandal et. al. 2014)

Condition	Specific Heat
Without filler	3.967 J/g K at 200°C and 2.383 J/g K at -23°C
With filler	2.635 J/g K at 200°C and 1.565 J/g K at -23°C

The flow chart below shows the summary of parametric study at different combinations

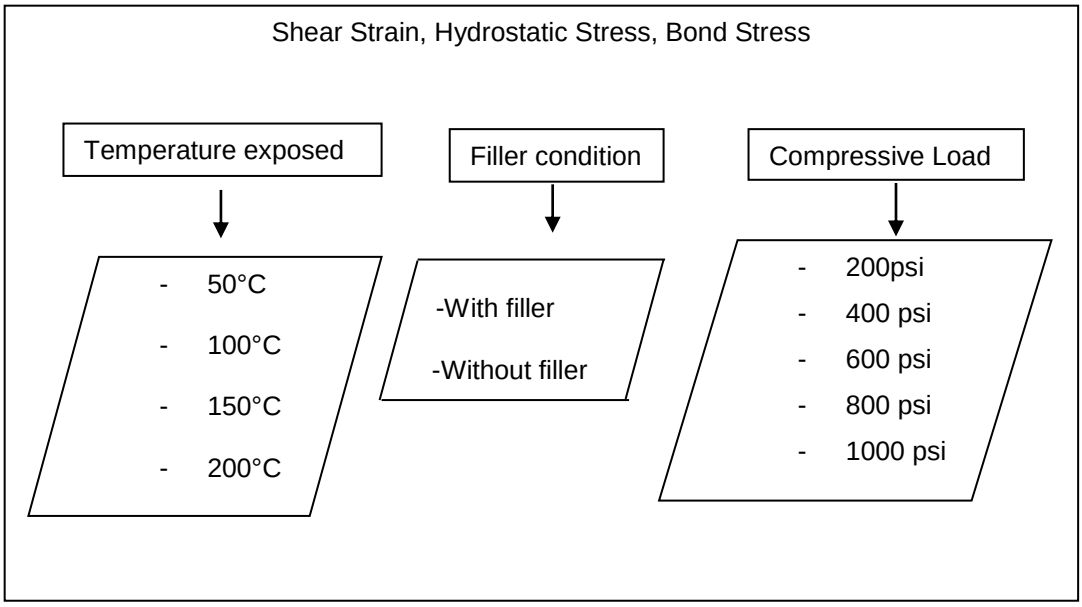

The bearing pad is exposed to a temperature range of 25 to 200°C as shown in Figure 5-18. Temperature is assumed to reach its maximum by 60 seconds as it was the case in the fire test. The temperature is modelled using radiation and conductive heat transfer for 3600 seconds. This time scale is selected so that it is close to the thermocouple data time record in fire experiment.

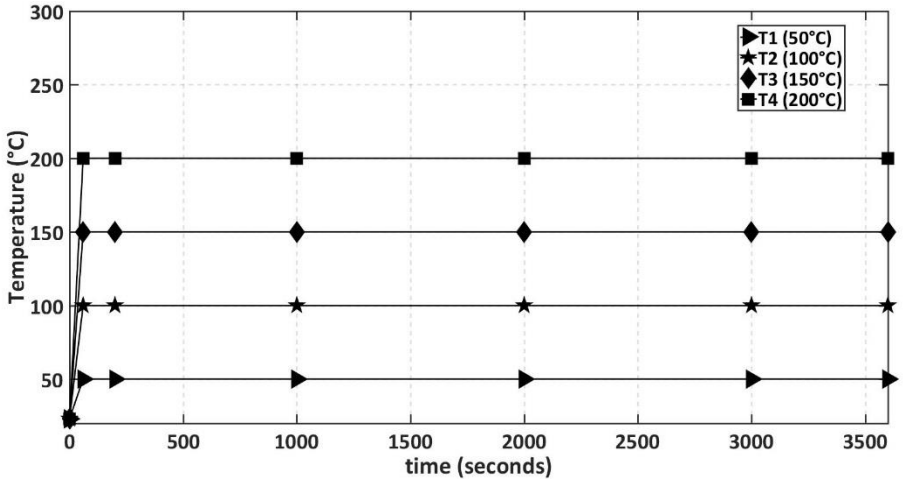

Figure 5-18 Exposed Temperatures

After exposing the bearing pad to different ranges of temperatures, the variation of nodal temperature along the width of bearing pad is shown in Figure 5-19. For example, when the bearing pad is exposed to 100°C for 3600 seconds the exterior face of bearing pad along the width has developed a temperature about 77°C, and in the interior the nodal temperature drops rapidly. Hence the change in nodal temperature especially in interior nodes is less compared to nodes near the face.

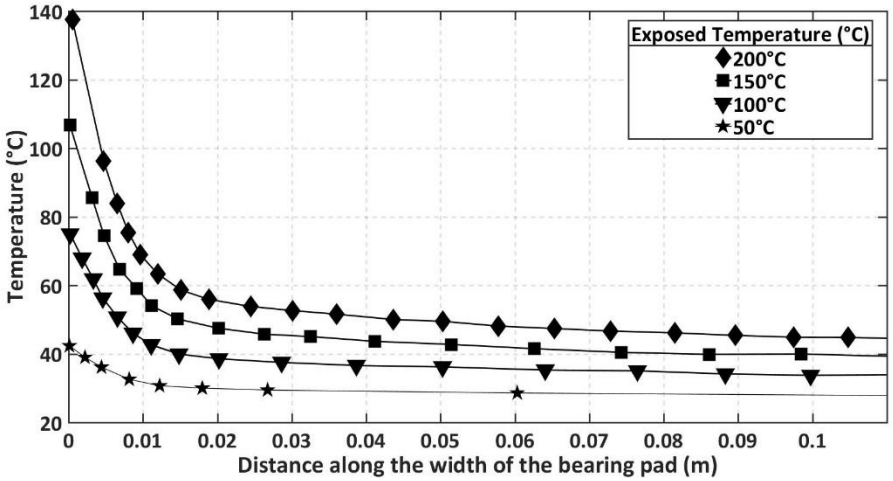

Figure 5-19 Temperature Variation along the width of the bearing pad (at t =3600 sec.)

The main parameters that are of interest are: shear strain, bond stress and hydrostatic tensile stress. Table 5-17 to Table 5-21 shows the variation of these parameters before and after exposing the bearing pad to different temperatures.

The effect of different parameters on performance of bearing pad are discussed below-

5.3.1 Shear Strain

There is a significant change in shear strain when exposed to different temperatures on different grades of elastomer. The change in shear strain depends on factors as applied compressive stress, temperature exposed, presence of filler and the grade of elastomer. Detailed explanation on change of shear strain based on each parameter is presented below –

5.3.1.1 Effect of temperature

As temperature increased the shear strain also increased. Its value almost doubled when temperature increased from 23° to 50°C, increase was about 107%. But at 200°C the increase is only by 142% compared to shear strain at ambient temperature, as shown in Table 5-17. This is because of low thermal conductivity of elastomer which insulates the interior parts to the external changes in temperature. Hence, the low thermal conductivity of elastomer in a way was advantageous from performance point of view.

As the grade of elastomer grade increased, the total shear strain decreased as shown from Table 5-17 to Table 5-19, especially mechanical strains as the elastomer modulus increased. Hence in the total shear the thermal strain contribution dominated for higher grades of elastomer. For 50 duro elastomer the increase in shear strain at 200°C

is 142% at 1.37MPa applied compressive stress. But for 70 duro elastomer the increase is 216%.

5.3.1.2 Effect of compressive stress applied

Total shear strain increased as the applied compressive stress increased. At higher compressive loads, the mechanical strains dominate the thermal strains. Hence at lower compressive stress and at 50°C exposed temperature the increase in shear strain is around 100% but as the applied stress increased the increase in shear strain has reduced to 15-30%.

Table 5-17 Effect of Temperature on Shear Strain – 50 DURO

Compressive Stress (MPa)	Shear Strain (m/m)					
	Exposed Temperature					AASHTO
	23°C (ambient) (% change from AASHTO)	50°C (% increase from 23°C)	100°C (% increase from 23°C)	150°C (% increase from 23°C)	200°C (% increase from 23°C)	
1.37 (200 psi)	0.38 (-15%)	0.79 (107%)	0.84 (121%)	0.86 (126%)	0.92 (142%)	0.45
2.75 (400 psi)	0.76 (-15.6%)	1.17 (54%)	1.22 (60%)	1.27 (67%)	1.31 (72%)	0.89
4.13 (600 psi)	1.16 (-13.4%)	1.57 (35%)	1.61 (38%)	1.65 (42%)	1.69 (46%)	1.34
5.51 (800 psi)	1.53 (-15%)	1.96 (28%)	2.01 (31%)	2.06 (34%)	2.1 (37%)	1.8
6.9 (1000 psi)	1.93 (-14.2%)	2.25 (16%)	2.32 (20%)	2.38 (23%)	2.42 (25%)	2.25

Table 5-18 Effect of Temperature on Shear Strain – 60 DURO

Compressive Stress (MPa)	Shear Strain (m/m)					
	Exposed Temperature					AASHTO
	23°C (ambient) (% change from AASHTO)	50°C (% increase from 23°C)	100°C (% increase from 23°C)	150°C (% increase from 23°C)	200°C (% increase from 23°C)	
1.37 (200 psi)	0.19 (-35%)	0.39 (105%)	0.44 (132%)	0.48 (153%)	0.53 (179%)	0.29
2.75 (400 psi)	0.38 (-35.3%)	0.6 (58%)	0.64 (68%)	0.68 (79%)	0.73 (92%)	0.58
4.13 (600 psi)	0.58 (-34.28)	0.79 (36%)	0.84 (45%)	0.87 (50%)	0.92 (59%)	0.88
5.51 (800 psi)	0.77 (-34.6%)	0.99 (29%)	1.05 (36%)	1.09 (42%)	1.12 (45%)	1.17
6.9 (1000 psi)	0.97 (-34.1%)	1.17 (21%)	1.22 (25%)	1.26 (29%)	1.31 (35%)	1.47

Table 5-19 Effect of Temperature on Shear Strain – 70 DURO

Compressive Stress (MPa)	Shear Strain (m/m)					
	Exposed Temperature					AASHTO
	23°C (ambient) (% change from AASHTO)	50°C (% increase from 23°C)	100°C (% increase from 23°C)	150°C (% increase from 23°C)	200°C (% increase from 23°C)	
1.37 (200 psi)	0.12 (-33.4%)	0.26 (116%)	0.29 (142%)	0.34 (183%)	0.38 (216%)	0.18
2.75 (400 psi)	0.24 (-33.6%)	0.38 (58%)	0.41 (71%)	0.45 (87%)	0.5 (108%)	0.36
4.13 (600 psi)	0.35 (-35.5%)	0.5 (43%)	0.54 (55%)	0.58 (66%)	0.62 (77%)	0.54
5.51 (800 psi)	0.47 (-35.13%)	0.62 (32%)	0.69 (47%)	0.7 (49%)	0.74 (57%)	0.72
6.9 (1000 psi)	0.59 (-34.8%)	0.78 (32%)	0.81 (37%)	0.83 (40%)	0.86 (46%)	0.9

5.3.1.4 Effect of fillers

The effect of shear strains due to the presence of fillers on different grades of elastomer are shown from Figure 5-20 to Figure 5-22. As it can be seen, there is no significant changes in shear strain due to presence of fillers. This is because, even though the thermal conductivity increased by 100% but specific heat also increased in same proportion. Hence the nodal temperatures didn't increase significantly due to increased specific heat of elastomer due to the presence of fillers.

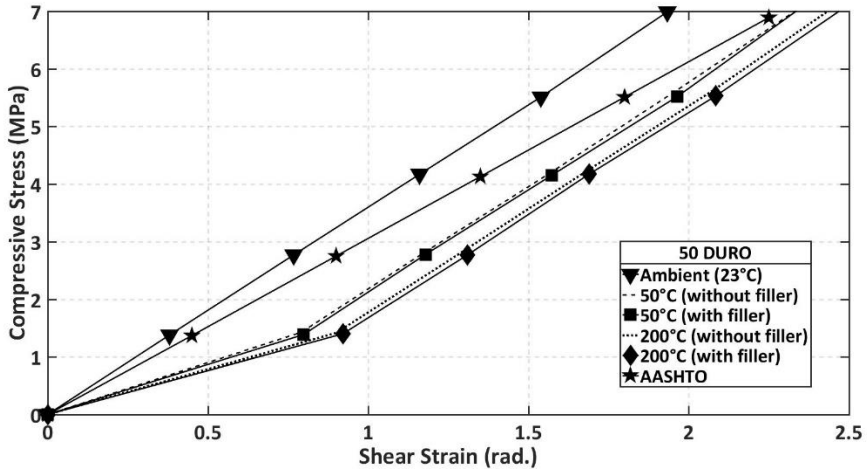

Figure 5-20 Effect of filler and temperature on 50 Duro elastomer bearing pad

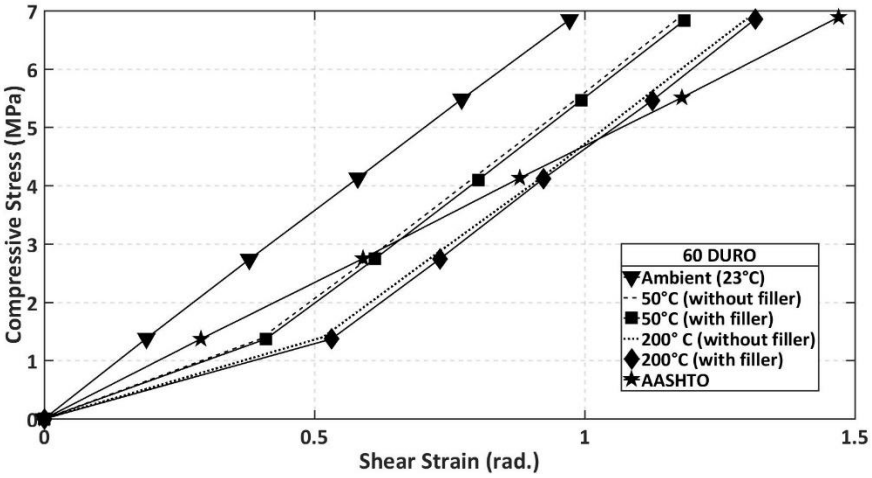

Figure 5-21 Effect of filler and temperature on 60 Duro elastomer bearing pad

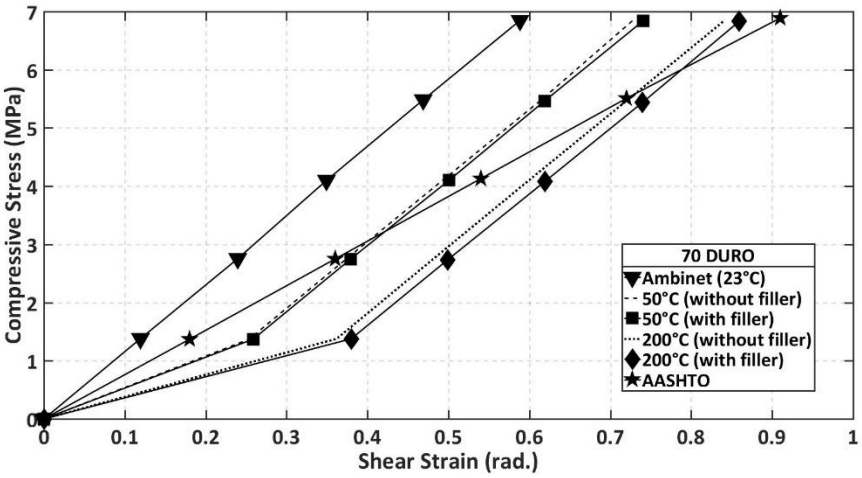

Figure 5-22 Effect of temperature and filler on 70 Duro elastomer bearing pad

5.3.2 Hydrostatic Stress

There is a significant change in hydrostatic stress when exposed to different temperatures on different grades of elastomer. The change hydrostatic stress depends on factors as applied compressive stress, temperature exposed, presence of filler and the grade of elastomer. Detailed explanation on change of hydrostatic stress based on each parameter is presented below –

5.3.2.1 Effect of temperature

As temperature increased the hydrostatic stress also increased as shown in Table 5-20. Its value doubled when temperature increased from 23° to 50°C. But at 200°C the increase is only by 128% compared to its value at ambient temperature. This is because of low thermal conductivity of elastomer which insulates the interior parts to the external changes in temperature. Hence the low thermal conductivity of elastomer in a way was advantageous from performance point of view.

Table 5-20 Effect of Temperature on Hydrostatic Stress

Compressive Stress (MPa)	Hydrostatic Tensile Stress (MPa)				
	Exposed Temperature				
	23°C (ambient)	50°C (% increase from 23°C)	100°C (% increase from 23°C)	150°C (% increase from 23°C)	200°C (% increase from 23°C)
1.37 (200 psi)	0.47	0.94 (100%)	0.98 (108%)	1.02 (117%)	1.07 (128%)
2.75 (400 psi)	0.92	1.42 (54%)	1.47 (60%)	1.51 (64%)	1.56 (69%)
4.13 (600 psi)	1.39	1.91 (37%)	1.96 (41%)	2 (44%)	2.05 (48%)
5.51 (800 psi)	1.88	2.35 (25%)	2.4 (27%)	2.45 (30%)	2.5 (33%)
6.9 (1000 psi)	2.32	2.8 (20.6%)	2.85 (23%)	2.9 (25%)	2.95 (27%)

5.3.2.2 Effect of compressive stress applied

As the externally applied compressive stress increased the hydrostatic stress also increased. At lower compressive stress and at 50°C exposed temperature the increase in shear strain is around 100% but as the applied stress increased the increase in shear strain has reduced to 20%. As temperature increased from 50°C to 200°C, the hydrostatic stress increased as discussed in previous section. This is because at higher compressive stress the mechanical strains dominate the thermally induced strains.

5.3.3 Bond Stress

Bond stress changed when exposed to different temperatures on different grades of elastomer. The change bond stress depends on factors such as applied compressive stress, temperature exposed, presence of filler and the grade of elastomer. Detailed explanation on change of bond stress based on each parameter is presented below.

5.3.3.1 Effect of temperature

As temperature increased the bond stress also increased as shown in Table 5-21. Its value increased by 140% when temperature increased from 23° to 50°C. But at 200°C the increase is only by 154% compared to its value at ambient temperature. This is because of low thermal conductivity of elastomer which insulates the interior parts to the external changes in temperature. Hence the low thermal conductivity of elastomer in a way was advantageous from performance point of view. Bond stress remained almost same for different grades of elastomer and presence of filler didn't have any significant effect as in the case of shear strain.

5.3.3.2 Effect of compressive stress applied

As the externally applied compressive stress increased the bond stress also increased. At lower compressive stress and at 50°C exposed temperature the increase in

bond stress is around 140% but as the applied stress increased the increase in shear strain has reduced to 27%. As temperature increased from 50°C to 200°C, the bond stress increased as discussed in previous section. This is because at higher compressive stress the mechanical strains dominate the thermally induced strains.

Most of the bond stress values are within the limit 1.31MPa except at 6.98MPa compressive load. So, failure due to increased bond stress is not of a concern as temperature increases.

Table 5-21 Effect of Temperature on Bond Stress

Compressive Stress (MPa)	Bond Stress (MPa)				
	Exposed Temperature				
	23°C (ambient)	50°C (% increase from 23°C)	100°C (% increase from 23°C)	150°C (% increase from 23°C)	200°C (% increase from 23°C)
1.37 (200 psi)	0.2	0.48 (140%)	0.5 (144.1%)	0.52 (148.3%)	0.55 (154.6%)
2.75 (400 psi)	0.4	0.73 (82%)	0.76 (90%)	0.78 (95%)	0.8 (100%)
4.13 (600 psi)	0.6	0.92 (53%)	0.94 (56%)	0.96 (60%)	0.99 (65%)
5.51 (800 psi)	0.8	1.09 (36%)	1.12 (40%)	1.15 (44%)	1.19 (49%)
6.9 (1000 psi)	0.99	1.26 (27%)	1.3 (31%)	1.34 (35%)	1.37 (38%)

Chapter 6

SUMMARY AND CONCLUSIONS

Temperature effect on elastomeric bearing pads is studied in this research. Temperature changes could lead to long term effects like creep due to aging and short-term effects as thermal expansion due to daily temperature variations. In all these cases effect of temperature on elastomer is required and there is no past research on the overall fire performance of bearing pad. Hence, the current research was conducted with the aim of bridging this knowledge gap. The research was divided into three phases. The first phase involved conducting a full-scale fire test, where bearing pads are exposed to fire for about one hour and tested for material properties after cooling down. The second phase was involved developing a thermo-mechanical numerical modeling scheme to study various performance parameters of elastomeric bearing pads. In third phase, a parametric study was conducted to the study the effect of temperature, presence of fillers and different grades of elastomer. The summary and conclusions of this research is discussed below.

6.1 Summary and conclusions

In the first phase of research the bearing pads are subjected to pool fire which lasted for one hour. The bearing pads were then tested for hardness, shear modulus, compression set and adhesion strength. All the samples for these experiments were taken from the exterior faces of bearing pad where the damage was worse. It was found that the experimental results were within the quality control limits except for compression set. Compression set value almost tripled for some samples, which means that the elastomer has lost its ability to recover to its original shape. But this property as

suggested by NCHRP 449 (2001) is not relevant to performance of bearing pads. To understand the long-term creep due to fire, a full-scale creep test must be performed. One of the most important property for bearing pad is its adhesion strength. But it was found that the adhesion strength values are within the limits even after the fire test. Hence, from these tests, it can be concluded that the bearing pads performed well in hydrocarbon pool fire. However, to understand the creep in elastomer due to heat, compression set value alone is not sufficient and a full-scale test is recommended.

In the second phase of the research, a numerical simulation was performed to study the performance parameters of bearing pad. The elastomer was modeled as linear elastic and as nonlinear elastic material. The results from both the models were compared with the AASHTO (2012) equations in finding shear strain produced under compression, shear and rotation. It was found out that the AASHTO (2012) values for shear strain are conservative. Nonlinear material model yielded much less shear strains at higher compressive loads than AASHTO (2012) values. Also, parameters such as bond stress, von Mises stress in steel, maximum principal strain and hydrostatic tensile stresses were studied under different material models for elastomer. All their values from both linear and nonlinear material models were within the limits recommended.

In the third phase of the research, a parametric study was conducted by varying the thermal properties of elastomer taking into account the presence of fillers and the modulus of elasticity of elastomer to account for different hardness grades such as 50, 60 and 70 Duro. The bearing pad was exposed to temperatures ranging from 50 to 200°C for one hour. The observations made were:

- Shear strain in elastomer increases significantly when temperature is increased.

- At higher compressive loads, the mechanical shear strain dominates the thermal shear strain.
- The contribution of thermal shear strain is more in the higher grades of elastomer.
- Hydrostatic tensile stress and bond stress didn't change significantly for different grades of elastomer.
- Hydrostatic stress and bond stress increased with temperature.
- Both hydrostatic stress and bond stress are within the limits at different temperatures and compressive loads considered in this study.

From the observations made from all phases of the research in can be concluded that:

- The will be significant thermal strains in bearing pad when exposed to temperature.
- The thermal strains produced depends on many factors such as temperature magnitude, grade of elastomer and applied compressive stress.

6.2 Impact on bridge engineering practice

The current research has found that there will be a significant increase in estimated shear strain in elastomer from AASHTO (2014) if thermally induced strains are to be accounted for. From the current research an additional shear strain of 0.4, 0.3, 0.2 can be added in addition to the shear strains due to mechanical deformations. Also as these thermally induced strains could of cyclic nature due to daily temperature variations. So, if treated as cyclic loads, magnification factor of 1.75 needs to be multiplied as per AASHTO (2014) provisions. Hence, thermal strains could have a significant contribution to the overall shear strain. But however, a parametric study needs to be performed on

different shapes of bearing pads and at different exposed time periods of temperature to have a more generalized estimate of thermally induced strains in elastomer.

From the full scale testing the maximum increase in shear modulus was found to be 26.43%. This value is very small to account for the beneficial effects of bearing pad due to shear stiffening on the bridge girder as suggested by Yazdani et al. (2000), which was around 50 times the initial shear modulus. Also at this increased value of shear modulus, the design of substructure for an 5% horizontal force would be adequate to account for the horizontal restraint in the beams.

6.3 Future research recommendations

The following are the recommendations for future work:

- In hyperelastic model of elastomer, the mechanical response of bearing pad depends on the material constants used. A sensitivity analysis could be done on those material constants to have more confidence on the results from numerical analysis.
- A parametric study could be conducted for bearing pads of different sizes and shapes.
- A detailed analysis could be performed on the thermal properties of different grades of elastomers, which has different filler content.
- The nodes on top and bottom surface of bearing pad many not be fixed as modeled in this research due to presence of friction between girder and bearing pad. So, a study could be performed to see the effect of boundary conditions on the performance of bearing pad.

References

1. AASHTO: M251-06 (2011). “Standard Specification for Plain and Laminated Elastomeric Bridge Bearings”.
2. AASHTO (2014). “AASHTO LRFD bridge design specification.” American Association of State Highway Transportation Officials.
3. Alan Wineman (2009). “On the mechanics of elastomers undergoing scission and cross-linking” International Journal of Advances in Engineering Sciences and Applied Mathematics, Volume 1, Issue 2, pp 123–131.
4. Alok Kumar (2000). “Performance related parameters of elastomeric bearings” PhD dissertation, Univ. of Texas at Austin.
5. Arunava Mandal, Sandip Pan, Subrata Mukherjee, Achintya K. Saha, Sabu Thomas, Asmita Sengupta (2014). “Variations in Specific Heat and Microstructure in Natural Rubber Filled with Different Fillers as Studied by Differential Scanning Calorimetry” Journal of Polymer and Biopolymer Physics Chemistry, 2014, Vol. 2, No. 1, 25-28.
6. ASDTR 61-234 (1962). “Handbook of Design Data on Elastomeric Materials Used in Aerospace Systems” Directorate of Materials and Process, Ohio.
7. ASTM D2240 – 15 “Standard Test Method for Rubber Property—Durometer Hardness”.
8. ASTM D4014 – “Standard Specifications for Plain and Steel Laminated Elastomeric Bearings for Bridges”.
9. ASTM D395 – Standard Test Methods for Rubber Property – Compression Set.”
10. ASTM D429 – “Standard Test Methods for Rubber Property – Adhesion to Rigid Substrates”.
11. “Bridge Bearings – a Historical Survey”, Volker Wetzk

<< http://www.arct.cam.ac.uk/Downloads/ichs/vol-3-3333-3356-wetzk.pdf>> Last accessed May 27th 2017.

12. Brown, R. P. (1996). “Physical Testing of Rubber”, Chapman & Hall, London, UK.
13. Committee for European Normalisation (CEN). EN 1991-1-2:2004 “Eurocode 2: design of concrete Structures-Part 1-2: general rules – structural fire design.” Brussels, Belgium.
14. Committee of European Normalisation (CEN) (1993–2005b), EN 1993-1-2-2005, Eurocode 3: Design of Steel Structures, Part 1-2: Structural Fire Design, CEN, Brussels.
15. Dorfmann, A., Pabst, O., Beha, R., (1999). “Combined numerical and experimental analysis of the mechanical and thermal stress distribution in a rubber-aluminum roll.” International Organization for the Study of Transportation by Rope; San Francisco, Calif.
16. Eyosias Beneberu (2016).“Hydrocarbon Pool Fire Performance of Fiber Reinforced Polymer (FRP) Strengthened and Thermally Insulated Bridges.” PhD dissertation, Univ. of Texas at Arlington.
17. Gent, A.N. (1964) “Elastic Stability of Rubber Compression Springs”. Jo. Mech. Engr Sci. 6(4), pp. 318-326.
18. Gent, A.N. and Lindley, P.B. (1959a). “Internal Rupture of Bonded Rubber Cylinders in Tension”. Royal Society of London, Series A, Vol. 249, pp 195-205.
19. Gent, A.N. and Lindley, P.B. (1959b). “The Compression of Bonded Rubber Blocks” Proc. Inst. Mech. Engrs. Vol. 173, pp111-222.
20. Gent A N, Tompkins DA (1969). “Nucleation and Growth of Gas Bubbles In Elastomers”, Journal of Applied Physics, v 40 n 6.

21. George B. K., Stewart W. Manson, Raymond B. S. (1990). “Happy and unhappy balls: Neoprene and polynorbornene” Products of Chemistry Vol. 67 No. 3.
22. Hubert Oggermüller (2008). “Effects of Fillers on the Thermal Conductivity of Elastomers” << http://www.hoffmann-mineral.com/content/download/282/2361/file/Effects+of+Fillers+on+the+Heat+Conductivity+of+Elastomer.pdf >> Last accessed May 28th 2017.
23. Isidoro Matrinez (2017).“Properties of Solids” << http://webserver.dmt.upm.es/~isidoro/dat1/eSol.pdf >> Last accessed May 29th 2017.
24. Jae-Hyeok Choi, Hee-Jin Kang, Hyun-Yong Jeong Tae-Soo Lee (2005). “Heat Aging Effects on the Material Property and the Fatigue Life of Vulcanized Natural Rubber, and Fatigue Life Prediction Equations” Journal of Mechanical Science and Technology (KSME Int. J.), VoL 19, No. 6; pp. 1229-1242, 2005 1229.
25. Materials Handbook – Cambridge Univ. Eng. Dept. and from Manufacturer.
26. Markmann, G. and E. Verron, (2005). Efficiency of Hyperelastic Models for Rubber-Like Materials. In: Constitutive Models for Rubber IV, Austrell, P.E. and L. Kari (Eds.). AA Balkema Publishers, UK., ISBN: 10: 0415383463, pp: 375-380.
27. McPherson, Archibald Turner & Kemin, Alexander (1956). “Engineering uses of rubber.” Reinhold, New York.
28. NCHRP 12-68 (2006). “Rotational Limits for elastomeric bearings.” Prepared for Transportation Research Board Of The National Academies.
29. NCHRP 449 (2001). “Elastomeric Bridge Bearings: Recommended Test Methods” Prepared for Transportation Research Board Of The National Academies. Washington, DC.

30. Quiel, S., Yokoyama, T., Bergman, L., Mueller, K and Marjanishvili, S. (2015). “A Streamlined Framework for Calculating the Response of Steel-supported Bridges to Open -air Tanker Truck Fires.” Fire Safety Journal. Volume 73, Pages 63-75.
31. SFPE (2016). “SFPE Handbook of fire protection engineering.” 5th Ed., SFPE, Quincy, Massachusetts.
32. Stanton, J.F., and Lund, H. (2006). "Effects of Bulk Compressibility on the Response of Elastomeric Bearings," accepted for publication, Journal of Structural Engineering, ASCE, Reston VA.
33. Smith, L.P., (1993). The Language of Rubber: An Introduction to the Specification and Testing of Elastomers. Butterworth-Heinemann Ltd., London, England, ISBN: 10: 0750614137, pp: 257
34. Tobolsky A.V., Mercurio (1959). A. “Stress relaxation studies of scission in rubber vulcanizates,” Journal of polymer science, Volume 36.
35. TxDOT Bearing Pad Design Example (2010). << https://ftp.dot.state.tx.us/pub/txdot-info/library/pubs/bus/bridge/rectangular_cap_ex.pdf >> Last accessed May 29th 2017.
36. Yazdani, N., Eddy, S., and Cai, S. C., (2000). “Effect of Bearing Pads on Precast Prestressed Concrete Bridges.” Journal of Bridges Engineering., 5(3), 224 – 232.
37. Yeoh, O. H. (1990). “Characterization of Elastic Properties of Carbon-Black-Filled Rubber Vulcanizates,” Rubber Chemistry and Technology, 63, 792.
38. Zacharey S Harper et. Al. (2013). Calculation method for quantifying axial and rolling stiffness for rectangular steel-reinforced elastomeric bridge bearing pads. Transportation Research Record: Journal of the Transportation Research Board ,Volume 2331.

Biographical Information

Shashank Malal received his Bachelor of Technology from National Institute of Technology Calicut, India in 2014. He worked as a design engineer and in project management services for the construction of Cochin International Terminal and other Govt. of Kerala projects. His area of interest includes – seismic design of high rise structures, precast construction, construction with sustainable materials.